

An Interactive Shader for Natural Diffraction Gratings

Bachelorarbeit

der Philosophisch-naturwissenschaftlichen Fakultät
der Universität Bern

vorgelegt von

Michael Single

2014

Leiter der Arbeit:
Prof. Dr. Matthias Zwicker
Institut für Informatik und angewandte Mathematik

Abstract

In nature color production is the result of physical interaction of light with a surface's nanostructure. In his pioneering work, Stam developed limited reflection models based on wave optics, capturing the effect of diffraction on very regular surface structures. We propose an adaption of his BRDF model such that it can handle complex natural gratings. On top of this, we describe a technique for interactively rendering diffraction effects, as a result of physical interaction of light with biological nanostructures such as snake skins. As input data, our method uses discrete height fields of natural gratings acquired by using atomic force microscopy (AFM). Based on Taylor Series approximation we leverages precomputation to achieve interactive rendering performance (about 5-15 fps). We demonstrate results of our approach using surface nanostructures of different snake species applied on a measured snake geometry. Lastly, we evaluate the quality of our method by a comparison of the maxima for peak viewing angles using the data produced by our method against the maxima resulting by the grating equation.

Contents

1	Introduction	1
1.1	Motivation	1
1.2	Goals	3
1.3	Previous work	4
1.4	Thesis Structure	5
2	Derivations	7
2.1	Problem Statement and Challenges	7
2.2	Approximate a FT by a DFT	8
2.2.1	Reproduce FT by DTFT	8
2.2.2	Spatial Coherence and Windowing	9
2.2.3	Reproduce DTFT by DFT	11
2.3	Adaption of Stam's BRDF discrete height fields	13
2.3.1	Rendering Equation	13
2.3.2	Reflected Radiance of Stam's BRDF	14
2.3.3	Relative Reflectance	15
2.4	Optimization using Taylor Series	17
2.5	Spectral Rendering	19
2.6	Alternative Approach	19
2.6.1	PQ factors	19
2.6.2	Interpolation	22
3	Implementation	23
3.1	Precomputations in Matlab	25
3.2	Java Renderer	27
3.3	GLSL Diffraction Shader	29
3.3.1	Vertex Shader	29
3.3.2	Fragment Shader	31
3.4	Technical details	34
3.4.1	Texture lookup	34
3.4.2	Texture Blending	36
3.4.3	Color Transformation	36
3.5	Discussion	36
A	Signal Processing Basics	39
A.1	Fourier Transformation	39
A.2	Convolution	41
A.3	Taylor Series	41

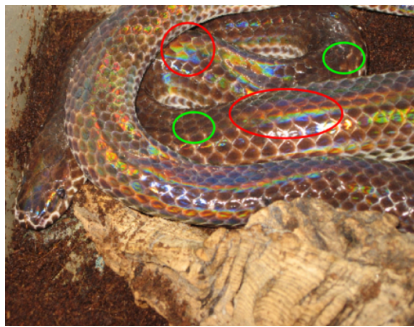
B Summary of Stam's Derivations	42
C Summary of Stam's Derivations	45
C.1 Taylor Series Approximation	45
C.1.1 Proof Sketch of 1.	45
C.1.2 Part 2: Find such an N	45
C.2 PQ approach	47
C.2.1 One dimensional case	47
C.2.2 Two dimensional case	49
D Appendix	50
D.1 The 3rd component w	50
D.2 Schlick's approximation	50
D.3 Spherical Coordinates	51
D.4 Tangent Space	51
List of Tables	53
List of Figures	53
List of Algorithms	54
Bibliography	55

Chapter 1

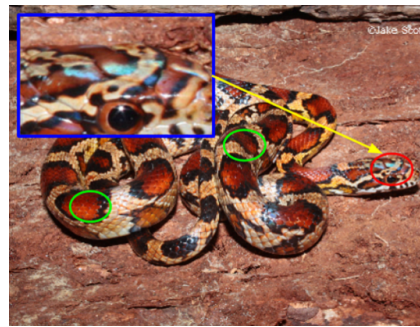
Introduction

1.1 Motivation

As human beings, we visually perceive and experience our whole world in terms of colors, resulting from various physical phenomena involving interaction between light and matter. Particularly in nature, there are basically two main causes for color production. Firstly, due to pigmentation, which occurs since certain molecules in a biological structure selectively absorb or reflect specific wavelengths from an incident light source. And secondly because of structural colors which are the result of physical interaction of light with a nanostructure, exclusively relying on the structuring of the material and not any other property. A natural diffraction grating is a semitransparent layer of biological nano-structures which exhibits a certain degree of regularity to produce structural colors by diffracting an incident light source. One particular example for such biological color production are the colors we can see when having a closer look at the illuminated skin of snakes, as shown in figure 1.1.



(a) Xenopeltis snake



(b) Elaphe Guttata snake

Figure 1.1: Examples of pigmentation color (green circles) and structural color (red circles) on different snake species¹.

¹image source of figure 1.1(a) http://www.snakes-alive.co.uk/gallery_5.html and figure 1.1(b) http://www.the-livingrainforest.co.uk/living/view_price.php?id=464

Some species like *Xenopeltis* express structural colors in form of iridescent patterns along their scales way stronger than others like *Elaphe* species. The reason for this lies on the nanostructure of their skins. There are a vast amount of additional reasons for producing structural colors in nature, such as thin film interference, intra-cellular photonic crystals or diffraction gratings. More detailed examples are shown in figure 1.2.

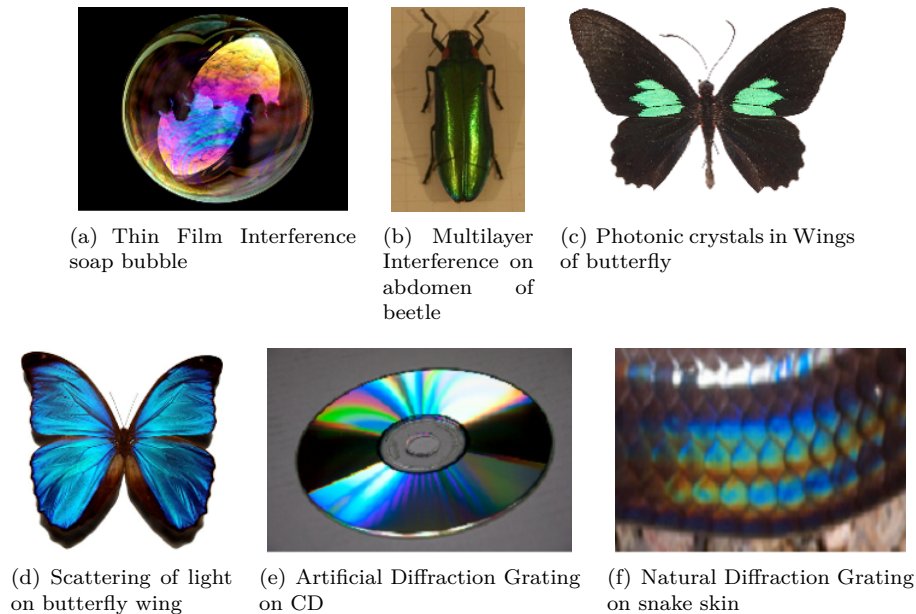


Figure 1.2: Examples² for structural colors on the wings and the abdomen of insects, liquids, synthetic structures, and on scales on the skin of reptiles.

As far back as in the 17th century, Robert Hooke was able to relate the cause of structural colors to the microstructure of a material. During his examinations of peacock feathers he found that the colors could be made disappear by wetting the feathers and further observed that the feathers are made of tiny ridges. Building on top of the latest knowledge about interference, Newton related structural colors with wave interference. Recently, in the field of computer graphics, many researchers have developed models to render structural colors, but most of the currently available models are not able to perform interactive rendering or are oversimplified and thus cannot model accurately the effect of diffraction.

²image source of figure:

- 1.2(a): http://www.ualberta.ca/~pogosyan/teaching/PHYS_130/FALL_2010/lectures/lect33/lecture33.html
- 1.2(b): <http://www.itp.uni-hannover.de/~zawischa/ITP/multibeam.html>
- 1.2(c): http://upload.wikimedia.org/wikipedia/commons/a/a4/Parides_sesostriis_MHNT_dos.jpg
- 1.2(d): From paper [MT10], figure 6.
- 1.2(e): <http://cnx.org/content/m42496/latest/?collection=col11428/latest>
- 1.2(f): http://www.snakes-alive.co.uk/gallery_5.html

This thesis investigates this particular problem in detail and provides a solution for rendering structural colors due to diffraction on natural gratings.

1.2 Goals

The purpose of this thesis is firstly, to simulate physically accurate structural colors caused by the effect of diffraction on various biological structures and secondly implement this simulation as a renderer with interactive behaviour. We mainly focus on structural colors generated by natural diffraction gratings. In particular the approach presented in this thesis applies to surfaces with quasiperiodic structures at the nanometer scale which can be represented as height fields stored in gray-scale images.

Natural gratings like this are found on the scale of reptiles, wings of butterflies or the bodies of various insects but we restrict ourself and focus on snake skins. The data of our discrete valued height fields, which are representing the surface of a measured snake skin was acquired using atomic force microscopy (AFM)³. Figure 1.3 shows a measured height field of a *Xenopeltis* snake, which stored in a grayscale image. The surface of its skin is composed of many finger like structures. Locally, these fingers seem to be very regularly aligned (red box). However, globally, we observe that the alignment of the fingers is irregularly curved (indicated by green curves) along the whole surface. This kind of global irregularity is why it makes it hard to model the structural complexity of natural gratings⁴.

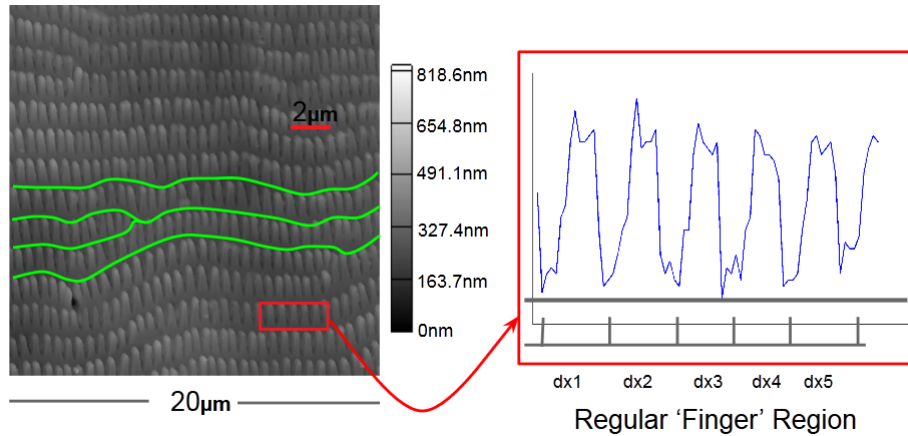


Figure 1.3: Height field of a *Xenopeltis* snake⁵ skin taken by AFM and stored as a grayscale image. Locally, this natural grating consists of regularly aligned (red box) finger-like substructures, but globally we observe a curved alignment of these structures (green curves).

³All data is provided by the Laboratory of Artificial and Natural Evolution in Geneva. See their website: www.lanevol.org

⁴E.g. by relying on statistical methods, capturing surface details by introducing an appropriate distribution function of the finger structures.

The renderer discussed in this thesis is based on the pioneering work of J. Stam about diffraction shaders [Sta99] in which he formulated a BRDF modelling the effect of diffraction. Nevertheless we have to adapt his BRDF model since his model assumes, that a given surface of a grating can either be formulated by an analytical function, and therefore has a closed form solution or it is simple enough to be modelled effectively by relying on statistical methods. However, we are dealing with natural diffraction gratings, represented as explicitly formulated height fields, which unfortunately are neither known analytically nor do they fit into simple statistical models. This thesis thus proposes an extension of J. Stam's work for the complex case of explicitly defined, discrete and quasi-periodic height field structures.

In the following section a brief overview of previous work relevant and related to this work will be presented.

1.3 Previous work

The first scientific descriptions of structural colors was previously by Hooke in 1665 in his book *Micrographia* [R.H12]. Hooke investigated feathers of peacocks using one of the first microscopes from his time and found out that the colors on the feather were canceled out whenever a drop of water moistened the feather. He proposed the speculation that a layer of thin plates and air were responsible for reflecting the light and thus he related the structure of the feather to colors. In Newton's book *Opticks* [I.N14] he described that the colors of the peacock feather are related to the thinness of the transparent part of the feathers. Around 1800 T.Young explains structural colors as a result of wave interference using his double-slit experiment⁶ [T.Y07], published in the journal *Philosophical Transactions of the Royal Society*.

In the field of computer graphics, J.Stam [Sta99] was the first one who was able to develop reflection models based on wave optics capturing the effect of diffraction due to nano-structure height fields. His model is an approximation of far field diffraction⁷ effects relying on the Kirchhof integral⁸. For a certain class of surfaces which can be modelled as a height field he provides an analytical solution of the BRDF model. He assumes homogeneity of the structure and then the main idea of his model is the formulate a BRDF as the Fourier Transform applied on the the correlation function of the given height field. However, the height fields that Stam is dealing with are either extremely regular or can be considered as a superposition of randomly distributed bumps forming a periodic like structure relying on probabilistic distribution theory⁹. Both height field assumptions allow him to derive an analytical solution using statistical models. However, the height field we are dealing with are measured, complex, biological nano-structures and thus they do not exhibit regularity at a global scale as demonstrated in figure 1.3. It is not sufficient to superimpose one particu-

⁵This image was provided by the LANE lab in Geneva

⁶See http://en.wikipedia.org/wiki/Double-slit_experiment

⁷See http://en.wikipedia.org/wiki/Fraunhofer_diffraction

⁸See http://en.wikipedia.org/wiki/Kirchhoff_integral_theorem

⁹See http://en.wikipedia.org/wiki/Probability_distribution

lar nano finger (considering it as a bump) for capturing the complexity of the measured structure since this poses a non-trivial problem of modeling the distribution of nano finger statistically. Therefore, we cannot directly use Stam's BRDF model when we want to perform interactive rendering for diffraction effects of natural gratings.

In 2012 Cuypers et al [CT12] proposed a wave based Bidirectional scattering distribution function (BSDF¹⁰) denoted as WBSDF. Using the rendering equation and Wigner Distribution Functions¹¹ (WDF) they related their WBSDF model to the incoming wavefront and hence, their model can be adapted such that it can be rendered by a Monte Carlo renderer. The advantage of their model over Stam's is that their models also captures near field diffraction effects. A disadvantage their model is computational expensive since the WDF of a two dimensional surface is a four dimensional function and therefore can hardly be used in order to perform interactive rendering.

Linday and Agu [CT12] proposed an approach in order to perform interactive rendering diffraction effect by precomputing and storing their BRDF model using spherical harmonics. Nonetheless, for complex natural gratings their BRDF may be insufficient accurate since their approach is using low order spherical harmonics.

1.4 Thesis Structure

The reminder of this thesis is organised as follows: Due to the fact that this thesis has a rather advanced mathematical complexity, chapter 2 introduces some important definitions about modelling light in computer graphics and some wave theory. These concept are required in order to be able to follow our later derivations. This is followed by a brief summary of J. Stam's Paper about diffraction shaders, since his BRDF formulation is the basis of our derivations.

In chapter 3 we adapt Stam's BRDF model step-wise in a way that we will end up with a representation which can be implemented as an interactive diffraction renderer when using natural diffraction gratings. We also propose an alternative formulation, the so called PQ approach in this chapter and discuss its short-comings.

Chapter 4 addresses the practical part of this thesis, the implementation of our diffraction model, explaining all precomputation steps and how rendering is preformed in our reference framework for this thesis.

Chapter 5 gives some further insight about diffraction by explaining the topic about diffraction grating in depth. Furthermore, within this chapter we evaluate the qualitative validity of our BRDF model applied on different surface gratings by computing their reflectance and comparing the results to the grating equation under similar conditions.

¹⁰See http://en.wikipedia.org/wiki/Bidirectional_scattering_distribution_function

¹¹See http://en.wikipedia.org/wiki/Wigner_distribution_function

Chapter 6 presents our rendered results, first the so called BRDF maps for all our gratings and shading approaches under various shading parameters and then the actual renderings on a snake skin. And finally chapter 7 contains the conclusion of this thesis discussing what has been achieved in this thesis and all the drawbacks of the proposed method. It also contains a note about some of my personal experiences during this thesis.

Chapter 2

Derivations

2.1 Problem Statement and Challenges

The goal of this thesis is to perform a physically accurate and interactive simulation of structural colors production like shown in figure 2.2, which we can see whenever a light source is diffracted on a natural grating. For this purpose we need to be provided by the following input data as shown in figure 2.1:

- A mesh representing a snake surface¹ with associated texture coordinates as shown in figure 2.1(a).
- A natural diffraction grating represented as a height field, its maximum height and its pixel-width-correspondence².
- A vectorfield which describes how fingers on a provided surface of the nanostructure are aligned as shown in figure 2.1(c).

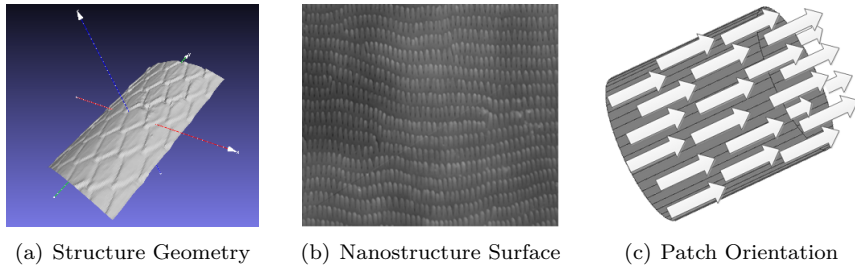


Figure 2.1: Input for our simulation

We want to rely on the integral equation ?? derived by J. Stam in his paper [Sta99] about diffraction shaders. This equation formaltes a BRDF modeling

¹Which is in our simulation an actual reconstruction of a real snake skin. These measurements are provided by the Laboratory of Artificial and Natural Evolution at Geneva. See their website: www.lanevol.org.

²Since the nanostructure is stored as a grayscale image, we need a scale telling us what length and height one pixel cooresponds to in this provided image.

the effect of diffraction under the assumption that a given grating can either be formulated as an analytical function or its structure is simple enough being modeled relying on statistical methods. These assumptions guarantee that ?? has an explicit solution. However, the complexity of a biological nanostructures cannot sufficiently and accurately modeled simply using statistical methods. This is why interactive computation at high resolution becomes a hard task, since we cannot evaluate the given integral equation on the fly. Therefore, we have to adapt Stam's equation such that we are able to perform interactive rendering using explicitly provided height fields.

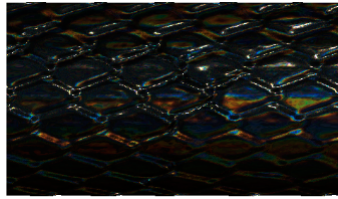


Figure 2.2: Output: Rendered Structural Colors

2.2 Approximate a FT by a DFT

2.2.1 Reproduce FT by DTFT

In the previous section, we have found an identity for the reflected spectral radiance $L_\lambda(\omega_r)$ when using Stam's BRDF for a given input height field. However, the derived expression in equation 2.12 requires to evaluate the Fourier Transform of our height field³ for every direction. In this section we explain how to approximate the FT by the DTFT and apply it to our previous derivations. Figure 2.3 graphically shows how to obtain the DTFT from the FT for a one dimensional signal⁴

The first step is to uniformly discretize the given signal since computers are working finite, discrete arithmetic. We rely on the Nyquist–Shannon sampling theorem tells us how dense we have to sample a given signal $s(x)$ such that can be reconstructed its sampled version $\hat{s}[n]$ ⁶. In particular, a sampled version according to the Nyquist–Shannon sampling theorem will have the same Fourier Transform as its original signal. The sampling theorem states that if f_{max} denotes the highest frequency of $s(x)$, then, it has to be sampled by a rate of f_s with $2f_{max} \leq f_s$ in order to be reconstructable. By convention $T = \frac{1}{f_s}$ represent the interval length between two samples.

³actually it requires the computation of the inverse Fourier Transform of a transformed version of the given heightfield, the function $p(x,y)$ defined in equation ??.

⁴For our case we are dealing with a two dimensional, spatial signal, the given height field. Nevertheless, without any constraints of generality, the explained approach applies to multi dimensional problems.

⁵Images of function plots taken from http://en.wikipedia.org/wiki/Discrete_Fourier_transform and are modified.

⁶ n denotes the number of samples.

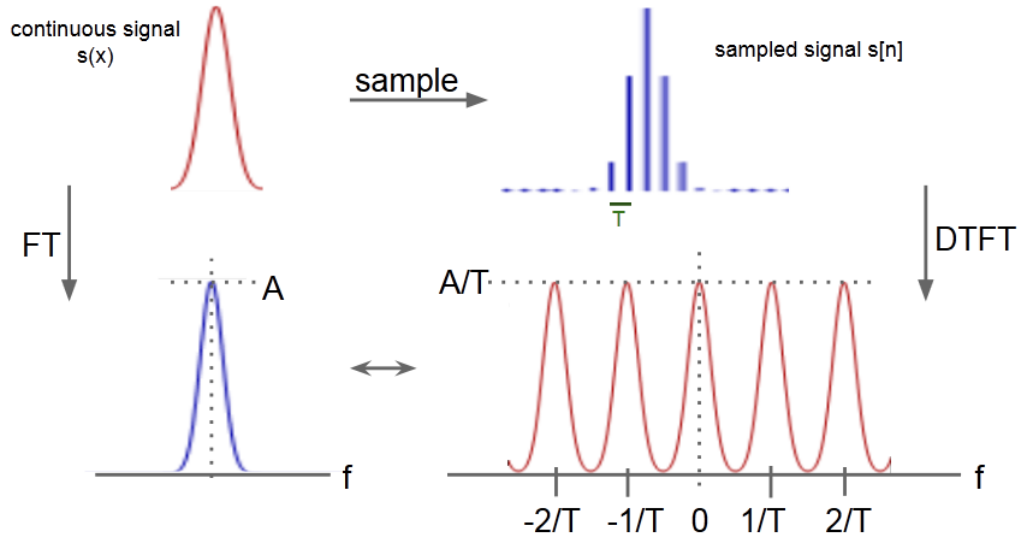


Figure 2.3: Illustration of how to approximate the analytical Fourier Transform (FT) ⁵ of a given continuous signal by a Discrete Time Fourier Transform (DTFT). The DTFT applied on a bandlimited, discretized signal yields a continuous, periodic response in frequency space.

Next, we apply the Fourier Transformation operator on the discretized signal \hat{s} which gives us the following expression:

$$\begin{aligned}
 \mathcal{F}_{FT}\{\hat{s}\}(w) &= \int_{\mathbb{R}} \hat{s}[n]e^{-iwx}dx \\
 &= \int_{\mathbb{R}} \text{mask}(x)s(x)e^{-iwx}dx \\
 &= T \sum_{x=-\infty}^{\infty} \hat{s}[x]e^{-iwx} \\
 &= T\mathcal{F}_{DTFT}\{s\}(w)
 \end{aligned} \tag{2.1}$$

Equation 2.1 tells us that if \hat{s} is sufficiently sampled, then its DTFT corresponds to the FT of $s(x)$. Notice that the resulting DTFT from the sampled signal has a height of $\frac{A}{T}$ where A is the height of the FT of s and thus is a scaled version of the FT.

2.2.2 Spatial Coherence and Windowing

Before we can derive a final expression in order to approximate a FT by a DFT, we first have to revisit the concept of coherence introduced in section ?? of chapter 2. Previously we have seen that Stam's BRDF tells us what is the total contribution of all secondary sources which allows us to say what is the reflected spectral radiance at a certain point in space. This is related to

stationary interference which itself depends on the coherence property of the emitted secondary wave sources. The ability for two points in space, t_1 and t_2 , to interfere in the extend of a wave when being averages over time is the so called spatial coherence. The spatial distance between such two points over which there is significant interference is limited by the quantity coherence area. For filtered sunlight on earth this is equal to $65\mu m$ ⁷.

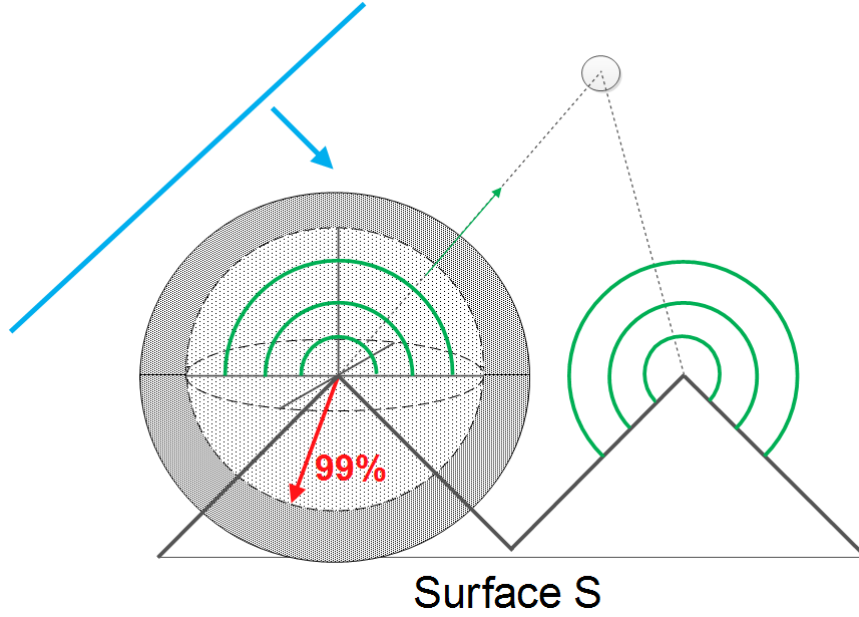


Figure 2.4: A plane wave encounters a surface. According to Huygens principle, secondary wavelets are emitted off from this surface. The resulting wave at a certain point in space (here indicated by a gray circle) depends on the interference among all waves encountering at this position. The amount of significant interference is directly affected by the spatial coherence property of all the wavelets.

Figure 2.4 illustrates the concept of spatial coherence. A wavefront (blue line) encounters a surface. Due to Hugen's Principle, secondary wavelets are emitted off from the surface. The reflected radiance at a certain point in space, e.g. at a viewer's eye position (denoted by the gray circle), is a result of interference among all wavelets at that point. This interference is directly affected by the spatial coherence property of all the emitted wavelets.

In physics spatial coherence is predicted by the cross correlation between t_1 and t_2 and usually modeled by a Gaussian Random Process. For any such Gaussian Processes we can use a spatial gaussian window $g(x)$ which is equal:

$$g(x) = \frac{1}{\sqrt{2\pi} \cdot \sigma} \cdot e^{-\frac{x^2}{2\sigma^2}} \quad (2.2)$$

⁷A proof for this number can be looked up in the book Optical Coherence and Quantum Optics[LM95] on page 153 and 154.

We have chosen standard deviation σ_s of the window such that it fulfills the equation $4\sigma_s = 65\mu m$. This is equivalent like saying we want to predict about 99.99%⁸ of the resulting spatial coherence interference effects in our model by a cross correlation function.

By applying the Fourier Transformation to the spatial window we get the corresponding window in frequency space will look like:

$$G(f) = e^{-\frac{f^2}{2\sigma_s^2}} \quad (2.3)$$

Notice that this frequency space window has a standard deviation σ_f equal to $\frac{1}{2\pi\sigma_s}$. Those two windows, the spatial- and the frequency space window, will be used in the next section in order to approximate the DTFT by the DFT by a windowing approach.

2.2.3 Reproduce DTFT by DFT

In this section we explain how and under what assumptions the DTFT of a discretized signal⁹ can be approximated by a DFT. The whole idea how to reproduce the DTFT by DFT is schematically illustrated in figure 2.5.

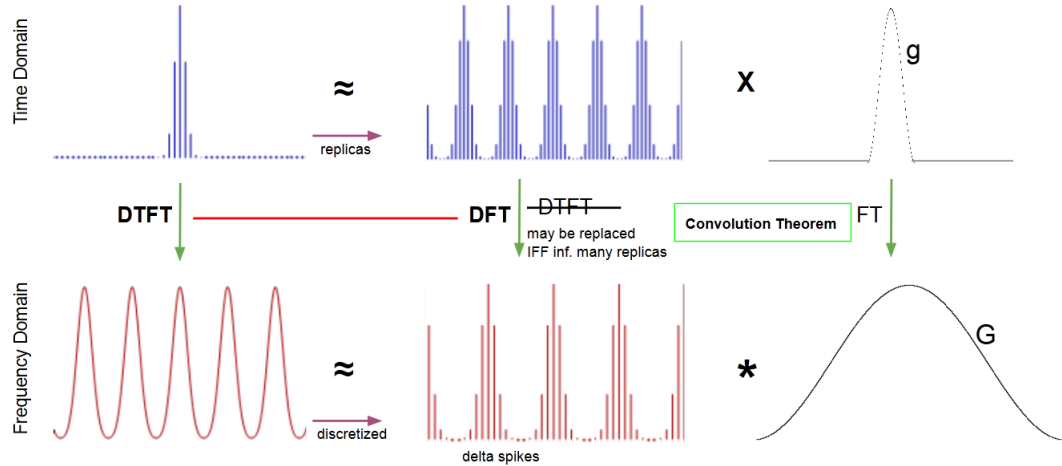


Figure 2.5: Illustration of how to approximate the DTFT¹⁰ by the DFT relying on the Convolution Theorem, using a gaussian window function.

Given a spatial, bandlimited and discretized one dimensional signal \hat{s} . Our goal is to approximate this spatial signal in a way such that when taking the DTFT of this approximated signal, it will yield almost the same like taking the DTFT of the original sampled \hat{s} . For this purpose we will use the previous

⁸Standard deviation values from confidence intervals table of normal distribution provided by Wolfram MatheWorld <http://mathworld.wolfram.com/StandardDeviation.html>.

⁹E.g. a sampled signal like already presented in figure 2.3

¹⁰Images of function plots taken from http://en.wikipedia.org/wiki/Discrete_Fourier_transform and are modified. Note that the scales in the graphic are not appropriate.

introduced concept of gaussian windows and the so called Convolution Theorem which is a fundamental property of all Fourier Transformations.

The Convolution Theorem states that the Fourier Transformation of a product of two functions, f and g , is equal to convolving the Fourier Transformations of each individual function. Mathematically, this statement corresponds to equation 2.4:

$$\mathcal{F}\{f \cdot g\} = \mathcal{F}\{f\} * \mathcal{F}\{g\} \quad (2.4)$$

The principal issue is how to approximate our given signal \hat{s} . Therefore, let us consider another signal \hat{s}_N which is the N times replicated version of \hat{s} (blue signal at center top in figure).

Remember that in general, the signal response at a certain point in space is the result of interference among all signals meeting at that position. In our scenario, the source of those signals are emitted secondary wavelets. The interference strength between these points is related to their spatial coherence. Windowing the signals by a gaussian window g will capture a certain percentage of all interference effects. From the previous section 2.2.2 we know that we can use gaussian window like in equation 2.2 in order to approximate such spatial signals interference effects.

Using this insight, we can approximate \hat{s} by taking the product of \hat{s}_N with a gaussian window g . This fact is illustrated in the first row of figure 2.3. So what will the DTFT of this approximation yield? We already know that the DTFT of \hat{s} is a continuous, periodic signal, since \hat{s} is bandlimited. Thus, taking the DTFT of this found approximation should give us approximatively the same continuous, periodic signal.

This is where the convolution theorem comes into play: Applying the DTFT to the product of \hat{s}_N and g is the same as convolving the DTFT of \hat{s}_N by DTFT of g . From equation 2.3 we already know that the DTFT of g is just another gaussian, denoted by G . On the other hand the DTFT of \hat{s}_N yields a continuous, periodic signal. The higher the value of N , the sharper the signal gets (denoted by delta spiked) and the closer it converges toward to the DFT. This is why the DFT is the limit of a DTFT applied on periodic and discrete signals. Therefore, for a large number of N we can replace the DTFT by the DFT operator when applied on \hat{s}_N .

Lastly, we see that the DTFT of \hat{s} is approximatively the same like convolving a gaussian window by the DFT of \hat{s}_N . This also makes sense, since convolving a discrete, periodic signal (DFT of \hat{s}_N) by a continuous window function G yields a continuous, periodic function.

In practise, we cannot compute the DTFT A.3 numerically due to finite computer arithmetic and hence working with the DFT is our only option. Furthermore, there are numerically fast algorithms in order to compute the DFT values of a function, the Fast Fourier Transformation (FFT). The DFT A.4 of a discrete height field is equal to the DTFT of an infinitely periodic function

consisting of replicas of the same height field. Not, let a spatial gaussian window g having a standard deviation for which $4\sigma_s$ is equal μm . Then, from before, it follows:

$$\mathcal{F}_{dtft}\{\mathbf{s}\} \equiv \mathcal{F}_{dft}\{\mathbf{s}\} * G(\sigma_f) \quad (2.5)$$

Therefore we can deduce the following expression from this:

$$\begin{aligned} \mathcal{F}_{dtft}\{\mathbf{t}\}(u, v) &= \int_{-\infty}^{\infty} \int_{-\infty}^{\infty} F_{dft}\{\mathbf{t}\}(w_u, w_v) \phi(u - w_u, v - w_v) dw_u dw_v \\ &= \int_{-\infty}^{\infty} \int_{-\infty}^{\infty} \sum_i \sum_j F_{dft}\{\mathbf{t}\}(w_u, w_v) \\ &\quad \delta(w_u - w_i, w_v - w_j) \phi(u - w_u, v - w_v) dw_u dw_v \\ &= \sum_i \sum_j \int_{-\infty}^{\infty} \int_{-\infty}^{\infty} F_{dft}\{\mathbf{t}\}(w_u, w_v) \\ &\quad \delta(w_u - w_i, w_v - w_j) \phi(u - w_u, v - w_v) dw_u dw_v \\ &= \sum_i \sum_j F_{dft}\{\mathbf{t}\}(w_u, w_v) \phi(u - w_u, v - w_v) \end{aligned} \quad (2.6)$$

where

$$\phi(x, y) = \pi e^{-\frac{x^2 + y^2}{2\sigma_f^2}} \quad (2.7)$$

2.3 Adaption of Stam's BRDF discrete height fields

2.3.1 Rendering Equation

As already discussed in the theoretical background chapter, colors are associated to radiance. Since we are starting with Stam's BRDF¹¹ formulation but want to perform a simulation rendering structural colors, we have to reformulate this BRDF equation such that we will end up with an identity of the reflected spectral radiance. This is where the rendering equation comes into play. Lets assume we have given an incoming light source with solid angle ω_i and θ_i is its angle of incidence, ω_r is the solid angle for the reflected light. Further let λ denote the wavelength¹² and Ω is the hemisphere of integration for the incoming light. Then, we are able to formulate a $BRDF_\lambda$ by using its definition ??:

¹¹Remember that a BRDF is the portion of a incident light source reflected off a given surface towards a specified viewing direction.

¹²Notice that, to keep our terms simple, we have dropped all λ subscripts for spectral radiance quantities.

$$\begin{aligned}
f_r(\omega_i, \omega_r) &= \frac{dL_r(\omega_r)}{L_i(\omega_i)\cos(\theta_i)d\omega_i} \\
\Rightarrow f_r(\omega_i, \omega_r)L_i(\omega_i)\cos(\theta_i)d\omega_i &= dL_r(\omega_r) \\
\Rightarrow \int_{\Omega} f_r(\omega_i, \omega_r)L_i(\omega_i)\cos(\theta_i)d\omega_i &= \int_{\Omega} dL_r(\omega_r) \\
\Rightarrow \int_{\Omega} f_r(\omega_i, \omega_r)L_i(\omega_i)\cos(\theta_i)d\omega_i &= L_r(\omega_r)
\end{aligned} \tag{2.8}$$

The last equation is the so called rendering equation . We assume that our incident light is a directional, unpolarized light source like sunlight and therefore its radiance is given as

$$L_{\lambda}(\omega) = I(\lambda)\delta(\omega - \omega_i) \tag{2.9}$$

where $I(\lambda)$ is the intensity of the relative spectral power for the wavelength λ . By plugging the identity in equation 2.9 into our current rendering equation 2.8, we will get:

$$\begin{aligned}
L_{\lambda}(\omega_r) &= \int_{\Omega} BRDF_{\lambda}(\omega_i, \omega_r)L_{\lambda}(\omega_i)\cos(\theta_i)d\omega_i \\
&= BRDF_{\lambda}(\omega_i, \omega_r)I(\lambda)\cos(\theta_i)
\end{aligned} \tag{2.10}$$

where $L_{\lambda}(\omega_i)$ is the incident radiance and $L_{\lambda}(\omega_r)$ is the radiance reflected by the given surface. Note that the integral in equation 2.10 vanishes since $\delta(\omega - \omega_i)$ is only equal one if and only if $\omega = \omega_i$.

2.3.2 Reflected Radiance of Stam's BRDF

We are going to use Stam's main derivation (??) for the $BRDF(\omega_i, \omega_r)$ in 2.10 by applying the fact that the wavenumber is equal $k = \frac{2\pi}{\lambda}$:

$$\begin{aligned}
BRDF(\omega_i, \omega_r) &= \frac{k^2 F^2 G}{4\pi^2 A w^2} \langle |P(ku, kv)|^2 \rangle \\
&= \frac{4\pi^2 F^2 G}{4\pi^2 A \lambda^2 w^2} \langle |P(ku, kv)|^2 \rangle \\
&= \frac{F^2 G}{A \lambda^2 w^2} \left\langle \left| P\left(\frac{2\pi u}{\lambda}, \frac{2\pi v}{\lambda}\right) \right|^2 \right\rangle
\end{aligned} \tag{2.11}$$

Going back to equation 2.10 and plugging equation 2.11 into it, using the definition of equation ?? and the equation D.1 for ω we will get the following:

$$\begin{aligned}
L_{\lambda}(\omega_r) &= \frac{F^2(1 + \omega_i \cdot \omega_r)^2}{A \lambda^2 \cos(\theta_i) \cos(\theta_r) \omega^2} \left\langle \left| P\left(\frac{2\pi u}{\lambda}, \frac{2\pi v}{\lambda}\right) \right|^2 \right\rangle \cos(\theta_i) I(\lambda) \\
&= I(\lambda) \frac{F^2(1 + \omega_i \cdot \omega_r)^2}{\lambda^2 A \omega^2 \cos(\theta_r)} \left\langle \left| P\left(\frac{2\pi u}{\lambda}, \frac{2\pi v}{\lambda}\right) \right|^2 \right\rangle
\end{aligned} \tag{2.12}$$

Note that the Fresnel term F is actually a function of (w_i, w_r) , but in order to keep the equations simple, we omitted its arguments. So far we just plugged Stam's BRDF identity into the rendering equation and hence have not significantly deviated from his formulation. Keep in mind that P denotes the Fourier transform of the provided height field which depends on the viewing and incidence light direction. Thus this Fourier Transform has to be recomputed for every direction which will slow down the whole computation quite a lot¹³. One particular strategy to solve this issue is to approximate P by the Discrete Fourier Transform (DFT)¹⁴ and separate its computation such that terms for many directions can be precomputed and then later retrieved by look ups. The approximation of P happens in two steps: First we approximate the Fourier Transform by the Discrete Time Fourier Transform (DTFT) and then, afterwards, we approximate the DTFT by the DFT. For further about basics of signal processing and Fourier Transformations please consult the appendix A.

Using the insight gained by equation 2.1 allows us to further simplify equation 2.12:

$$\begin{aligned} L_\lambda(\omega_r) &= I(\lambda) \frac{F^2(1 + \omega_i \cdot \omega_r)^2}{\lambda^2 A w^2 \cos(\theta_r)} \left\langle \left| P\left(\frac{2\pi u}{\lambda}, \frac{2\pi v}{\lambda}\right) \right|^2 \right\rangle \\ &= I(\lambda) \frac{F^2(1 + \omega_i \cdot \omega_r)^2}{\lambda^2 A w^2 \cos(\theta_r)} \left\langle \left| T^2 P_{dtft}\left(\frac{2\pi u}{\lambda}, \frac{2\pi v}{\lambda}\right) \right|^2 \right\rangle \end{aligned} \quad (2.13)$$

Where P_{dtft} is a substitute for $\mathcal{F}_{DTFT}\{s\}(w)$. Furthermore T the sampling distance for the discretization of $p(x, y)$ assuming equal and uniform sampling in both dimensions x and y .

2.3.3 Relative Reflectance

In this section we are going to explain how to scale our BRDF formulation such that all of its possible output values are mapped into the range $[0, 1]$. Such a relative reflectance formulation will ease our life for later rendering purposes since usually color values are within the range $[0, 1]$, too. Furthermore, this will allow us to properly blend the resulting illumination caused by diffraction with a texture map.

Let us examine what $L_\lambda(\omega_r)$ will be for a purely specular surface, for which $\omega_r = \omega_0 = \omega_i$ such that $\omega_0 = (0, 0, 1)$. For this specular reflection case, the corresponding radiance will be denoted as $L_\lambda^{spec}(\omega_0)$. When we know the expression for $L_\lambda^{spec}(\omega_0)$ we would be able to compute the relative reflected radiance for our problem 2.12 by simply taking the fraction between $L_\lambda(\omega_r)$ and $L_\lambda^{spec}(\omega_0)$ which is denoted by:

$$\rho_\lambda(\omega_i, \omega_r) = \frac{L_\lambda(\omega_r)}{L_\lambda^{spec}(\omega_0)} \quad (2.14)$$

¹³Even a fast variant of computation the Fourier Transform has a runtime complexity of $O(N \log N)$ where N is the number of sample.

¹⁴See appendix A for further information about different kinds of fourier transformations.

Notice that the third component w from the vector in equation ?? is squared equal $(\cos(\theta_i) + \cos(\theta_r))^{215}$. But first, let us derive the following expression:

$$\begin{aligned}
 L_\lambda^{spec}(\omega_0) &= I(\lambda) \frac{F(\omega_0, \omega_0)^2 (1 + \begin{pmatrix} 0 \\ 0 \\ 1 \end{pmatrix} \cdot \begin{pmatrix} 0 \\ 0 \\ 1 \end{pmatrix})^2}{\lambda^2 A (\cos(0) + \cos(0))^2 \cos(0)} \langle \left| T_0^2 P_{dtft}(0, 0) \right|^2 \rangle \\
 &= I(\lambda) \frac{F(\omega_0, \omega_0)^2 (1 + 1)^2}{\lambda^2 A (1 + 1)^2 1} \left| T_0^2 N_{sample} \right|^2 \\
 &= I(\lambda) \frac{F(\omega_0, \omega_0)^2}{\lambda^2 A} \left| T_0^2 N_{sample} \right|^2
 \end{aligned} \tag{2.15}$$

Where $N_{samples}$ is the number of samples of the DTFT A.3. Thus, we can plug our last derived expression 2.15 into the definition for the relative reflectance radiance 2.14 in the direction w_r and will get:

$$\begin{aligned}
 \rho_\lambda(\omega_i, \omega_r) &= \frac{L_\lambda(\omega_r)}{L_\lambda^{spec}(\omega_0)} \\
 &= \frac{I(\lambda) \frac{F(\omega_i, \omega_r)^2 (1 + \omega_i \cdot \omega_r)^2}{\lambda^2 A (\cos(\theta_i) + \cos(\theta_r))^2 \cos(\theta_r)} \langle \left| T_0^2 P_{dtft}(\frac{2\pi u}{\lambda}, \frac{2\pi v}{\lambda}) \right|^2 \rangle}{I(\lambda) \frac{F(\omega_0, \omega_0)^2}{\lambda^2 A} \left| T_0^2 N_{sample} \right|^2} \\
 &= \frac{F^2(\omega_i, \omega_r) (1 + \omega_i \cdot \omega_r)^2}{F^2(\omega_0, \omega_0) (\cos(\theta_i) + \cos(\theta_r))^2 \cos(\theta_r)} \langle \left| \frac{P_{dtft}(\frac{2\pi u}{\lambda}, \frac{2\pi v}{\lambda})}{N_{samples}} \right|^2 \rangle
 \end{aligned} \tag{2.16}$$

For simplification and better readability, let us introduce the following expression, the so called gain-factor:

$$C(\omega_i, \omega_r) = \frac{F^2(\omega_i, \omega_r) (1 + \omega_i \cdot \omega_r)^2}{F^2(\omega_0, \omega_0) (\cos(\theta_i) + \cos(\theta_r))^2 \cos(\theta_r) N_{samples}^2} \tag{2.17}$$

Using equation 2.17, we will get the following expression for the relative reflectance radiance from equation 2.16:

$$\rho_\lambda(\omega_i, \omega_r) = C(\omega_i, \omega_r) \langle \left| P_{dtft}(\frac{2\pi u}{\lambda}, \frac{2\pi v}{\lambda}) \right|^2 \rangle \tag{2.18}$$

Using the previous definition for the relative reflectance radiance equation 2.14:

$$\rho_\lambda(\omega_i, \omega_r) = \frac{L_\lambda(\omega_r)}{L_\lambda^{spec}(\omega_0)} \tag{2.19}$$

Which we can rearrange to the expression:

¹⁵Consult section D.1 in the appendix

$$L_\lambda(\omega_r) = \rho_\lambda(\omega_i, \omega_r) L_\lambda^{spec}(\omega_0) \quad (2.20)$$

Let us choose $L_\lambda^{spec}(\omega_0) = S(\lambda)$ such that it has the same profile as the relative spectral power distribution of CIE Standard Illuminant *D65* discussed in 3.4.3. Furthermore, when integrating over λ for a specular surface, we should get CIE_{XYZ} values corresponding to the white point for *D65*. The corresponding tristimulus values using CIE colormatching functions ?? for the CIE_{XYZ} values look like:

$$\begin{aligned} X &= \int_\lambda L_\lambda(\omega_r) \bar{x}(\lambda) d\lambda \\ Y &= \int_\lambda L_\lambda(\omega_r) \bar{y}(\lambda) d\lambda \\ Z &= \int_\lambda L_\lambda(\omega_r) \bar{z}(\lambda) d\lambda \end{aligned} \quad (2.21)$$

where \bar{x} , \bar{y} , \bar{z} are the color matching functions. Combining our last finding from equation 2.20 for $L_\lambda(\omega_r)$ with the definition of the tristimulus values from equation 2.21, allows us to derive a formula for computing the colors values using Stam's BRDF formula relying on the rendering equation 2.8. Without any loss of generality it suffices to derive an explicit expression for just one tristimulus term, for example Y , the luminance:

$$\begin{aligned} Y &= \int_\lambda L_\lambda(\omega_r) \bar{y}(\lambda) d\lambda \\ &= \int_\lambda \rho_\lambda(\omega_i, \omega_r) L_\lambda^{spec}(\omega_0) \bar{y}(\lambda) d\lambda \\ &= \int_\lambda \rho_\lambda(\omega_i, \omega_r) S(\lambda) \bar{y}(\lambda) d\lambda \\ &= \int_\lambda C(\omega_i, \omega_r) \left\langle \left| P_{dft} \left(\frac{2\pi u}{\lambda}, \frac{2\pi v}{\lambda} \right) \right|^2 \right\rangle S(\lambda) \bar{y}(\lambda) d\lambda \\ &= C(\omega_i, \omega_r) \int_\lambda \left\langle \left| P_{dft} \left(\frac{2\pi u}{\lambda}, \frac{2\pi v}{\lambda} \right) \right|^2 \right\rangle S(\lambda) \bar{y}(\lambda) d\lambda \\ &= C(\omega_i, \omega_r) \int_\lambda \left\langle \left| P_{dft} \left(\frac{2\pi u}{\lambda}, \frac{2\pi v}{\lambda} \right) \right|^2 \right\rangle S_y(\lambda) d\lambda \end{aligned} \quad (2.22)$$

Where we used the definition $S_y(\lambda) \bar{y}(\lambda)$ in the last step.

2.4 Optimization using Taylor Series

Our final goal is to render structural colors resulting by the effect of wave diffraction. So far, we have derived an expression which can be used for rendering. Nevertheless, our current equation 2.22 used for computing structural colors, cannot be used for interactive rendering, since P_{dft} had to be recomputed for every change in any direction¹⁶.

¹⁶viewing or incident light direction

In this section, we will address this issue and deliver an approximation for the Fourier Transformation of Stam's auxiliary function $p(x, y)$. This will allow us to separate P_{dtft} in a way such that some computational expensive terms can be precomputed. This derivation will rely on the definition of Taylor Series expansion like shown in equation A.8. Further, we will provide an error bound for our approximation approach for a given number of terms. Last, we will extend our current BRDF formula by the findings derived within this section.

Given $p(x, y) = e^{ikwh(x, y)}$ from Stam's Paper ?? where $h(x, y)$ is a given height field. Let t be complex number, and let us consider the power series expansion of the exponential function:

$$e^t = 1 + t + \frac{t^2}{2!} + \frac{t^3}{3!} + \dots = \sum_{n=0}^{\infty} \frac{t^n}{n!} \quad (2.23)$$

Further, let us define

$$t = t(x, y) = ikwh(x, y) \quad (2.24)$$

where i is the imaginary unit. For simplification, let us denote $h(x, y)$ as h . Then it follows by our previous stated identities:

$$\begin{aligned} e^t &= 1 + (ikwh) + \frac{1}{2!}(ikwh)^2 + \frac{1}{3!}(ikwh)^3 + \dots \\ &= \sum_{n=0}^{\infty} \frac{(ikwh)^n}{n!}. \end{aligned} \quad (2.25)$$

Please note that above's Taylor series is convergent for any complex valued number t . Thus, plugging equation 2.25 into the definition of $p(x, y)$ will give us:

$$p(x, y) = \sum_{n=0}^{\infty} \frac{(ikwh(x, y))^n}{n!} \quad (2.26)$$

Next, let us now compute the Fourier Transformation \mathcal{F} of equation 2.26 form above:

$$\begin{aligned} \mathcal{F}\{p\} &\equiv \mathcal{F}\left\{\sum_{n=0}^{\infty} \frac{(ikwh)^n}{n!}\right\} \\ &\equiv \sum_{n=0}^{\infty} \mathcal{F}\left\{\frac{(ikwh)^n}{n!}\right\} \\ &\equiv \sum_{n=0}^{\infty} \frac{(ikw)^n}{n!} \mathcal{F}\{h^n\} \end{aligned} \quad (2.27)$$

Where we have used the fact that the Fourier Transformation is a linear operator. Therefore, from equation 2.27 it follows: $P(\alpha, \beta) = \sum_{n=0}^{\infty} \frac{(ikw)^n}{n!} \mathcal{F}\{h^n\}(\alpha, \beta)$ for which $\mathcal{F}\{h^n\}(u, v)$.

Next we are going to look for an $N \in \mathbb{N}$ such that

$$\sum_{n=0}^N \frac{(ikwh)^n}{n!} \mathcal{F}\{h^n\}(\alpha, \beta) \approx P(\alpha, \beta) \quad (2.28)$$

is a good approximation. But first, the following two facts would have to be proven¹⁷:

1. Show that there exist such an $N \in \mathbb{N}$ s.t the approximation holds true.
2. Find a value for B s.t. this approximation is below a certain error bound, for example machine precision ϵ .

Using now our approximation for $P_{dft} = \mathcal{F}^{-1}\{p\}(u, v)$ for the tristimulus value Y , we will get:

$$\begin{aligned} Y &= C(w_i, w_r) \int_{\lambda} \left\langle P_{dft}\left(\frac{2\pi u}{\lambda}, \frac{2\pi v}{\lambda}\right) \right\rangle^2 S_y(\lambda) d\lambda \\ &= C(w_i, w_r) \int_{\lambda} \left| \sum_{n=0}^N \frac{(wk)^n}{n!} \mathcal{F}^{-1}\{i^n h^n\}\left(\frac{2\pi u}{\lambda}, \frac{2\pi v}{\lambda}\right) \right|^2 S_y(\lambda) d\lambda \end{aligned} \quad (2.29)$$

2.5 Spectral Rendering

As the last step of our series of derivations, we plug all our findings together to one big equation in order to compute the color for each pixel on our mesh in the CIE_{XYZ} colorspace. For any given height-field $h(x, y)$ representing a small patch of a nano structure of a surface and the direction vectors w_i and w_r from figure ?? the resulting color caused by the effect of diffraction can be computed like: Let

$$P_{\lambda}(u, v) = F_{dft}\{i^n h^n\}\left(\frac{2\pi u}{\lambda}, \frac{2\pi v}{\lambda}\right) \quad (2.30)$$

Then our final expression using our previous derivations will look like:

$$\begin{aligned} \begin{pmatrix} X \\ Y \\ Z \end{pmatrix} &= C(\omega_i, \omega_r) \int_{\lambda} \sum_{n=0}^N \frac{(wk)^n}{n!} \sum_{(r,s) \in \mathcal{N}_1(u,v)} |P_{\lambda}(u - w_r, v - w_s)|^2 \\ &\quad \phi(u - w_r, v - w_s) \begin{pmatrix} S_x(\lambda) \\ S_y(\lambda) \\ S_z(\lambda) \end{pmatrix} d\lambda \end{aligned} \quad (2.31)$$

where $\phi(x, y) = \pi e^{-\frac{x^2+y^2}{2\sigma_f^2}}$ is the Gaussian window 2.2.3.

2.6 Alternative Approach

2.6.1 PQ factors

In this section we are presenting an alternative approach to the previous Gaussian window approach 2.2.3 in order to solve the issue working with $DTFT$ instead the DFT . We assume, that a given surface S is covered by a number

¹⁷Please have a look in section C.1 in the appendix

of replicas of a provided representative surface patch f . In a simplified, one dimensional scenario, mathematically speaking, f is assumed to be a repetitive function, i.e. $\forall x \in \mathbb{R} : S(x) = S(x + nT)$, where T is its period and $n \in \mathbb{N}_0$. Thus, the surfaces can be written formally as:

$$S(x) = \sum_{n=0}^N f(x + nT) \quad (2.32)$$

What we are looking for is an identity for the Fourier Transform¹⁸ of our surface S , required in order to simplify the (X, Y, Z) colors from 2.29:

$$\begin{aligned} \mathcal{F}\{S\}(w) &= \int f(x) e^{iwx} dx \\ &= \int_{-\infty}^{\infty} \sum_{n=0}^N f(x + nT) e^{iwx} dx \\ &= \sum_{n=0}^N \int_{-\infty}^{\infty} f(x + nT) e^{iwx} dx \end{aligned} \quad (2.33)$$

Next, apply the following substitution $x + nT = y$ which will lead us to:

$$\begin{aligned} x &= y - nT \\ dx &= dy \end{aligned} \quad (2.34)$$

Plugging this substitution back into equation 2.33 we will get:

$$\begin{aligned} \mathcal{F}\{S\}(w) &= \sum_{n=0}^N \int_{-\infty}^{\infty} f(x + nT) e^{iwx} dx \\ &= \sum_{n=0}^N \int_{-\infty}^{\infty} f(y) e^{iwy - iwnT} dy \\ &= \sum_{n=0}^N e^{-iwnT} \int_{-\infty}^{\infty} f(y) e^{iwy} dy \\ &= \sum_{n=0}^N e^{-iwnT} \mathcal{F}\{f\}(w) \\ &= \mathcal{F}\{f\}(w) \sum_{n=0}^N e^{-iwnT} \end{aligned} \quad (2.35)$$

We used the fact that the exponential term e^{-iwnT} is a constant factor when integrating along dy and the identity for the Fourier Transform of the function f . Next, let us examine the series $\sum_{n=0}^N e^{-iwnT}$ closer:

¹⁸Remember that we are using the definition of Fourier Transform used in electrical engineering where \mathcal{F} actually corresponds to the inverse Fourier Transform.

$$\begin{aligned}
\sum_{n=0}^N e^{-uwnT} &= \sum_{n=0}^N (e^{-iwt})^n \\
&= \frac{1 - e^{iwt(N+1)}}{1 - e^{-iwt}}
\end{aligned} \tag{2.36}$$

We recognize the geometric series identity for the left-hand-side of equation 2.36. Mainly relying on trigonometric identities, equation 2.35 can further simplified to:

$$\mathcal{F}\{S\}(w) = (p + iq)\mathcal{F}\{f\}(w) \tag{2.37}$$

where p and q are defined like:

$$\begin{aligned}
p &= \frac{1}{2} + \frac{1}{2} \left(\frac{\cos(wTN) - \cos(wT(N+1))}{1 - \cos(wT)} \right) \\
q &= \frac{\sin(wT(N+1)) - \sin(wTN) - \sin(wT)}{2(1 - \cos(wT))}
\end{aligned} \tag{2.38}$$

Please notice, all derivation steps can be found in the appendix in section C.2.1.

Now lets consider our actual problem description. Given a patch of a nanoscaled sureface snake shed represented as a two dimensional heightfield $h(x, y)$. We once again assume that this provided patch is representing the whole surface S of our geometry by some number of replicas of itself. Therefore, $S(x, y) = \sum_{n=0}^N h(x + nT_1, y + mT_2)$, assuming the given height field has the dimensions T_1 by T_2 . In order to derive an identity for the two dimensional Fourier transformation of S we can similarly proceed like we did to derive equation 2.37.

$$\mathcal{F}\{S\}(w_1, w_2) = (p + iq)\mathcal{F}_{DTFT}\{h\}(w_1, w_2) \tag{2.39}$$

Where all derivation steps can be found in the appendix in section C.2.2 and we have defined

$$\begin{aligned}
p &:= (p_1p_2 - q_1q_2) \\
q &:= (p_1p_2 + q_1q_2)
\end{aligned} \tag{2.40}$$

For the identity of equation 2.39 we made use of Green's integration rule which allowed us to split the double integral to the product of two single integrations. Also, we used the definition of the 2-dimensional inverse Fourier transform of the height field function. We applied a similar substitution like we did in 2.34, but this time twice, once for x_1 and once for x_2 separately. The last step in equation 2.39, substituting with p and q in equation ?? will be useful later in the implementation. The insight should be, that the product of two complex numbers is again a complex number. We will have to compute the absolute value of $\mathcal{F}\{S\}(w_1, w_2)$ which will then be equal $(p^2 + q^2)^{\frac{1}{2}} |\mathcal{F}\{h\}(w_1, w_2)|$

2.6.2 Interpolation

In 2.6.1 we have derived an alternative approach when we are working with a periodic signal instead using the gaussian window approach from 2.2.3. Its main finding 2.39 that we can just integrate over one of its period instead iterating over the whole domain. Nevertheless, this main finding is using the inverse DTFT. Since we are using

We are interested in recovering an original analog signal $x(t)$ from its samples $x[n] =$

Therefore, for a given sequence of real numbers $x[n]$, representing a digital signal, its correspond continuous function is:

$$x(t) = \sum_{n=-\infty}^{\infty} x[n] \text{sinc} \left(\frac{t - nT}{T} \right) \quad (2.41)$$

which has the Fourier transformation $X(f)$ whose non-zero values are confined to the region $|f| \leq \frac{1}{2T} = B$. When $x[n]$ represents time samples at interval T of a continuous function, then the quantity $f_s = \frac{1}{T}$ is known as its sample rate and $\frac{f_s}{2}$ denotes the Nyquist frequency. The sampling Theorem states that when a function has a Bandlimit B less than the Nyquist frequency, then $x(t)$ is a perfect reconstruction of the original function.

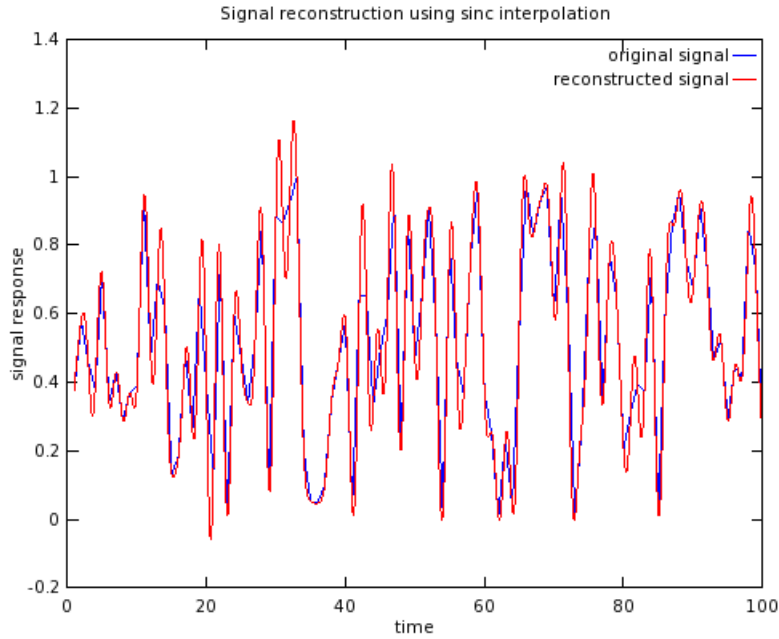


Figure 2.6: Comparission between a given random one dimensional input signal $s(t)$ and its sinc interpolation $\hat{s}(t)$. Notice that for the interpolation there were $N = 100$ samples from the original signal provided.

Chapter 3

Implementation

In computer graphics, we generally synthesize 2d images from a given 3d scene description. This process is denoted as rendering. Basically, rendering involves a mapping of 3d scene objects to a 2d image plane and the computation of each image pixel's color according to the provided lighting, viewing and material information of the given scene. These pixel colors are computed in several stages in so called shader programs, directly running on the Graphic Processing Unit (GPU) hardware device. In order to interact with a GPU, for our implementations, we rely on the programming interface of OpenGL¹, a cross-language, multiplatform API.

In OpenGL, there are two fundamental shading pipeline stages, the vertex- and the fragment shading stage, each applied sequentially.

In this chapter we explain in detail a technique for rendering structural colors due to diffraction effects on natural gratings, based on the model we have derived in the previous chapter 2, summarized in section 2.5. For this purpose we implemented a reference framework which is based on a class project of the lecture *Computer Graphics* held by Mr. M. Zwicker which I attended in autumn 2012².

Our implementation expects being provided by the following input data⁴:

- the structure of snake skin of different species⁵ represented as discrete valued height fields acquired using AFM and stored as grayscale images.
- real measured snake geometry represented as a triangle mesh.

gratings afm images, snake skin real measured snake geometry precomputations fourier terms in matlab there is implementation in java, based on framework

¹Official website:<http://www.opengl.org/>

²The code of underlying reference framework is written in Java and uses JOGL and GLSL³ in order to communicate with the GPU and can be found at <https://ilias.unibe.ch/>

³JOGL is a Java binding for OpenGL (official website <http://jogamp.org/jogl/www/>) and GLSL is OpenGL's high-level shading language. Further information can be found on wikipedia: http://de.wikipedia.org/wiki/OpenGL_Shading_Language

⁴All data is provided by the Laboratory of Artificial and Natural Evolution in Geneva. See their website:www.lanevol.org

⁵We are using height field data for Elaphe and Xenopeltis snakes individuals like shown in figure 1.1

In computergraphics, we generally synthesize 2d images from a given scene containing our 3d geometries by using so called shader programs. This process is denoted as rendering. The purpose of shader programs, which are executed directly on a GPU hardware device, is to compute the colorization and illumination of the objects present in our scene. All these computations happen in several stages and depend on the provided scene-input parameters like the camera, light sources, objects material constants and the desired rendering effect one is interested in to model. The shader stages are implemented sequentially as small little programs, the so called vertex-, geometry- and fragment-shaders. Those stages are applied within the rendering pipeline sequentially.

Our shaders which we use are written in a high-level language called GLSL, the OpenGL Shading Language. The decision for using OpenGL has been made since my underlying framework, which is responsible for the precomputation of all scene data, is based on another framework, written in Java using JOGL in order to communicate with the GPU and is also responsible to precompute all the relevant scene data. This framework, the so called jrtr framework, has been developed as an exercise during the class computer graphics held by M. Zwicker which I attended in autumn 2012. The framework itself has been used and extended during this thesis quite a lot. The DFT terms of the height field, required for rendering process in our framework is precomputed in Matlab. This is basically addressing all the required precomputations for the provided height-fields, referring to computation of the two dimensional Fourier Transformations which are further explained within this chapter. The Matlab scripts themselves rely on the provided snake nano-scaled sheds images, taken by AFM.

It's noteworthy that all the vertices and their associated data are processed within the vertex-shader, whereas the fragment shader's responsibility is to perform pixelwise rendering, using the input from the vertex shader. Just remember, fragments are determined by a triple of vertices. hence each pixel has assigned a trilinear interpolated value of all input parameters of its spanning vertices. Usually, all necessary transformations are applied vertex-wise, considering the vertex-shader as the preprocessing stage for the later rendering within the rendering pipeline, in the fragment-shader. In the geometry shader, new vertices around a considered vertex can be created. this is useful for debugging - displaying normals graphically for example.

In this part of thesis we are going to explain how we render our BRDF formulation derived in the last section in practice. All the necessary computations in order to simulate the effect of diffraction are performed within a fragment shader. This implies that we are modeling pixelwise the effect of diffraction and hence the overall rendering quality and runtime complexity depends on rendering window's resolution.

By the end of this chapter we will have seen how our render works and what we have to precompute.

3.1 Precomputations in Matlab

Our first task is to precompute the inverse two dimensional discrete Fourier transformations for a given snake shed patch of interest taken by AFM. For that purpose we have written a small Matlab script conceptualized algorithmically in 3.1. Matlab is a interpreted scripting language which offers a huge collection of mathematical and numerically fast and stable algorithms. Our Matlab script reads a given image, which is representing a nano-scaled height field, and computes its inverse two dimensional DFT by using Matlab's internal inverse fast Fourier Transformation function, denoted by *ifft2*. Note that we only require one color channel of the input image since the input image is representing an height field, encoded by just one color. Basically, we are interested in computing the *ifft2* for different powers of the input image times the imaginary number i since our taylor series approximation 2.4 relies on this. Keep in mind that taking the Fourier transformation of an arbitrary function will result in a complex valued output which implies that we will get a complex value for each pixel of our input image. Therefore, for each input image we get as many output images, representing the two dimensional inverse Fourier Transformation, as the minimal amount of taylor terms required for a well-enough approximation. In order to store our output images, we have to use two color channels instead just one like it was for the given input image. Some rendered images are shown in figure 3.1. Instead storing the computed values in plain images, we store our results in binary files. This allows us to have much higher precision for the output values and also it does not waste color channels. In our script every pixel value is normalized by its corresponding Fourier image extrema values such that it lays in the range $[0, 1]$. Therefore, we have to remember store four scaling factors for each output image as well. Those are the real and imaginary minimum and maximum values. Later, using linear interpolation within the shader, we will get back the rescaled image's original pixel values.

Algorithm 3.1 Precomputation: Pseudo code to generate Fourier terms

INPUT *heightfieldImg, maxH, dH, termCnt*

OUTPUT *DFT terms stored in Files*

```
% maxH:      A floating-point number specifying
%             the value of maximum height of the
%             height-field in MICRONS, where the
%             minimum-height is zero.
%
% dH:        A floating-point number specifying
%             the resolution (pixel-size) of the
%             'discrete' height-field in MICRONS.
%             It must be less than 0.1 MICRONS
%             to ensure proper response for
%             visible-range of light spectrum.
%
% termCnt:   An integer specifying the number of
%             Taylor series terms to use.

function ComputeFFTImages(heightfieldImg, maxH, dh, termCnt)
dh = dh*1E-6;
% load patch into heightfieldImg
patchImg = heightfieldImg.*maxH;
% rotate patchImg by 90 degrees
for t = 0 : termCnt
    patchFFT = power(1j*patchImg, t);
    fftTerm{t+1} = fftshift(fft2(patchFFT));

    % rescale terms as
    imOut(:, :, 1) = real(fftTerm{t+1});
    imOut(:, :, 2) = imag(fftTerm{t+1});
    imOut(:, :, 3) = 0.5;

    % rotate imOut by -90 degrees
    % find real and imaginary extrema of
    % write imOut, extrema, dH, into files.
end
```

The command `fftshift` rearranges the output of the `fft2` by moving the zero frequency component to the centre of the image. This simplifies the computation of lookup coordinates during rendering.

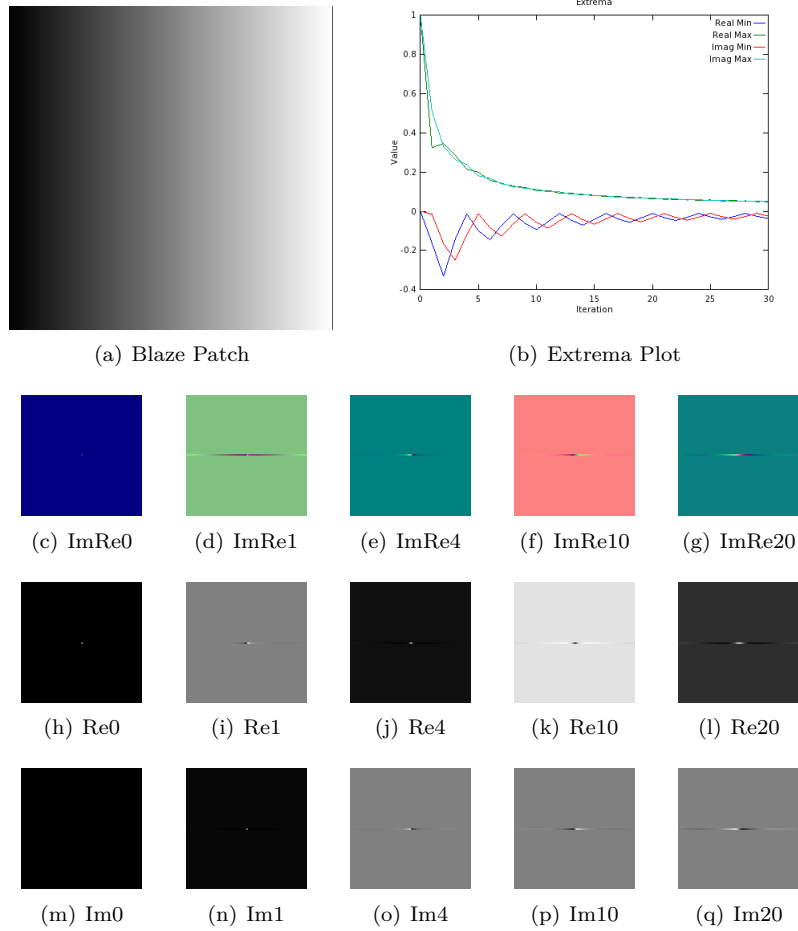


Figure 3.1: Blaze

In figure 3.1 we see some Fourier images rendered by our Matlab script for the blaze grating 3.1(a) used as input image. For example figure 3.1(e) represents the two dimensional Fourier transform of the input image to the power of four times the imaginary number i stored in a RGB image. Note that the red color channel 3.1(j) contains the real- and the green color channel 3.1(j) the imaginary part of the Fourier transform. The plot in figure 3.1(b) shows the development of blaze grating's extreme values for different powers.

3.2 Java Renderer

In autumn 2012, during the semester I have attended the class computer graphics held by M. Zwicker where we have developed a real time renderer program written in java. The architecture of the program is divided into two parts: a rendering engine, the so called jrtr (java real time renderer) and an application program. Figure 3.2 outlines the architecture of our renderer.

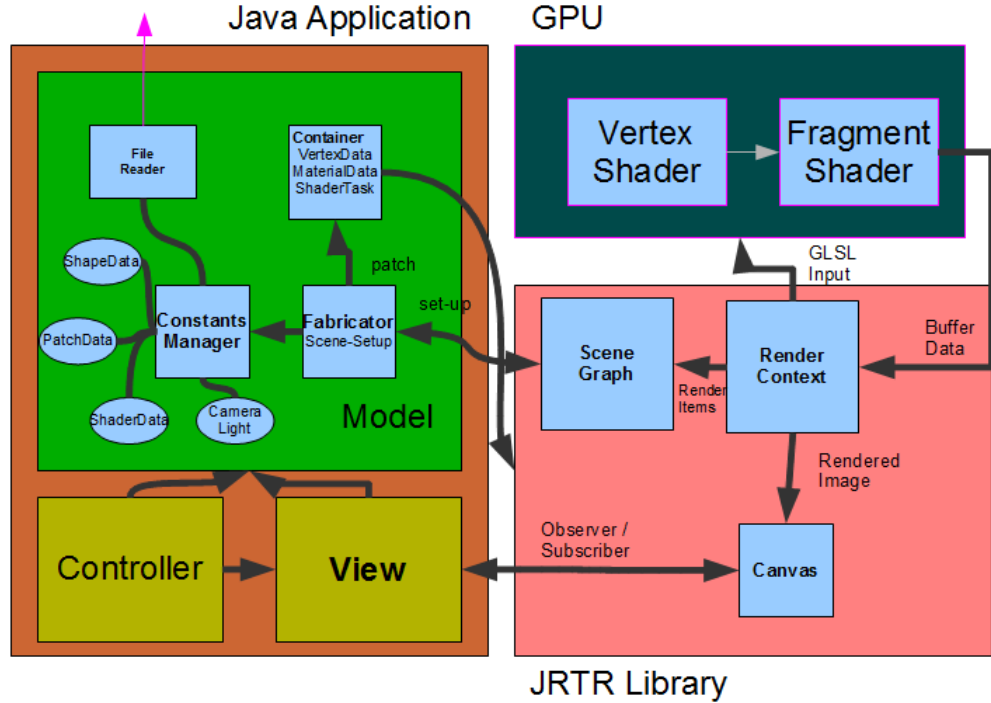


Figure 3.2: Renderer Architecture

The application program relies on the MVC (Model-View-Controller) architecture pattern. The View just represents a canvas in which the rendered images are shown. The Controller implements the event listener functionalities in order to manipulate the rendered shape within the canvas. The Model of our application program consists of a Fabricator, a file reader and a constants manager. The main purpose of a Fabricator is to set up a rendering scene by accessing a constant manager containing many predefined scene constants. A scene consists of a camera, a light source, a frustum, shapes and their associated material constants. Such materials contain a shape's texture, associated Fourier images *reffig : matlabBlazeFourierImages* for a given height field and other height field constants such as the maximal height of a bump. A shape is a geometrical object defined by a wireframe mesh as shown in figure 3.3.

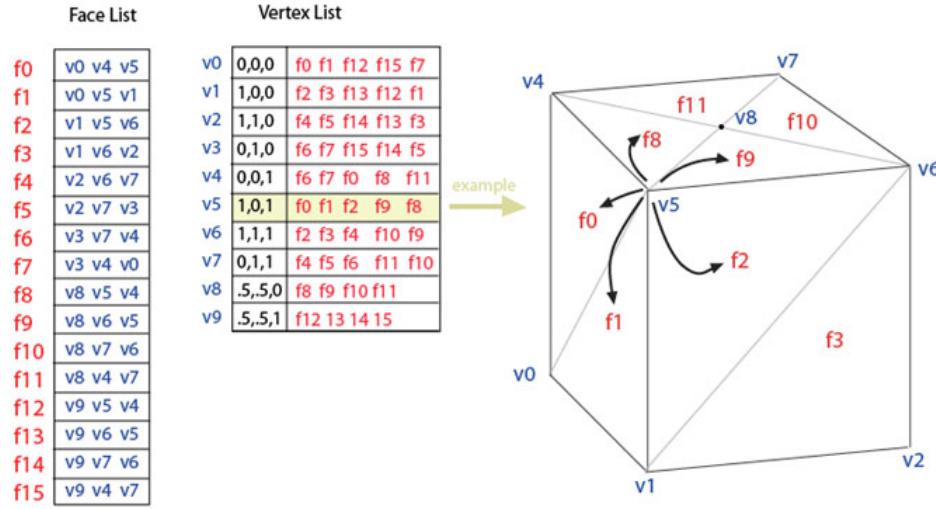


Figure 3.3: A wireframe mesh represents an object as a set of faces and a set of vertices.

Such a mesh is a special data structure consisting of vertices, each stored as a triple of xyz positions in an float array and triangles, each defined by a triple of vertex-indices which form a fragment each stored in an integer array. It is also possible to assign additional geometry data like a color, normals and texture coordinates associated to each vertex.

The whole scene is stored within container data-structures, defined and managed within jrtr. In our case we rely on a scene graph, which contains all geometries and their transformations in a tree like structured hierarchy. The geometries are stored within an container, including all vertex attributes and the material constants. The jrtr rendering engine uses a low-level API, called OpenGL in order to communicate with the graphics processor unit (GPU) where the actual shading happens. Within jrtr's render context object, the whole resource-management for the rendering pipeline takes place. This means all required low-level buffers are allocated, flushed and assigned by the scene data attributes. The GPU's rendering pipeline will use those buffers for its shading process. Its first stage is the vertex shader 3.3.1 followed by the fragment shader 3.3.2. The jrtr framework also offers the possibility to assign arbitrary shaders.

3.3 GLSL Diffraction Shader

3.3.1 Vertex Shader

The Vertex shader is the first shading stage within our rendering pipeline and responsible for computing all necessary per vertex data. Usually, within a vertex shader each vertex position is transformed into a projective space:

$$p_{projective} = P \cdot C^{-1} \cdot M \cdot p_{obj} \quad (3.1)$$

Where M is a transformation from the local object space to the reference coordinate system, called world space, C^{-1} camera matrix C and P the projection matrix. The camera matrix defines transformation from camera to world coordinates as shown in figure 3.4.

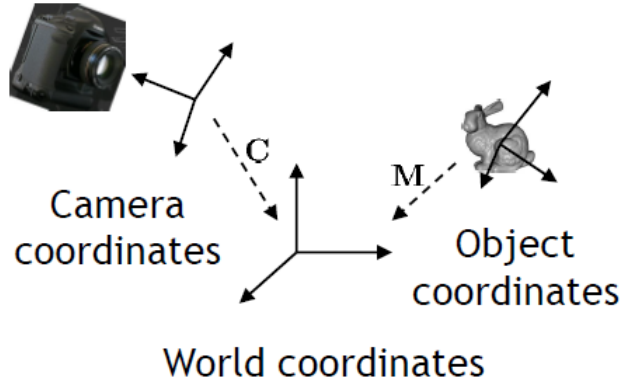


Figure 3.4: Camera coordinate system where its origin defines the center of projection of camera

The camera matrix is constructed from its center of projection e , the position the cameras looks at d and up vector denoted by up given in world coordinates like illustrated in figure 3.5

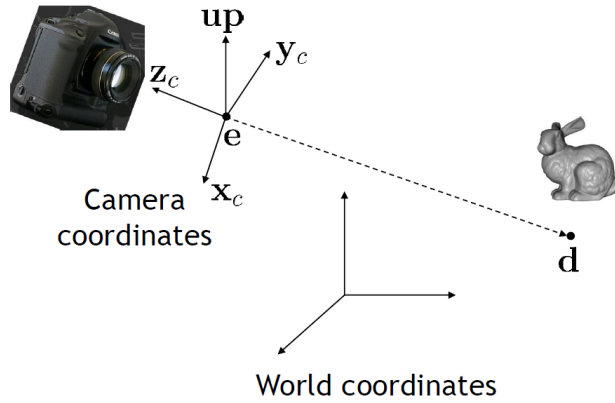


Figure 3.5: Illustration of involved components in order to construct the camera matrix. We introduce some helper vectors $z_c = \frac{e-d}{\|e-d\|}$, $x_c = \frac{up \times z_c}{\|up \times z_c\|}$ and $z_c \times x_c$ for the actual construction of the camera matrix

The mathematical representation of the camera matrix, using the helper vectors introduced in figure 3.5, looks like:

$$C = \begin{bmatrix} x_c & y_c & z_c & e \\ 0 & 0 & 0 & 1 \end{bmatrix} \quad (3.2)$$

All vertex shader output will be used within the fragment shader 3.3.2. In

our vertex shader we also compute for every vertex in our current geometry the direction vectors ω_i and ω_r described like in figure ???. Those direction vectors are transformed onto the tangent space, a local coordinate system spanned by a vertex's normal, tangent and binormal vector. Have a look at the appendix D.4 for further information and insight about the tangent space. The algorithm 3.2 stated below shows our vertex shader.

Algorithm 3.2 Vertex diffraction shader pseudo code

INPUT: $N, T, Shape, lightDir$

OUTPUT: $StructuralColoronFragment$

```

Foreach Vertex  $v \in Shape$  do
   $vec3\ N = normalize(modelM * vec4(normal, 0.0).xyz)$ 
   $vec3\ T = normalize(modelM * vec4(tangent, 0.0).xyz)$ 
   $vec3\ B = normalize(cross(N, T))$ 
   $vec3\ Pos = ((cop_w - position).xyz)$ 
   $lightDir = normalize(lightDir)$ 
   $l = projectVectorOnTo(lightDir, TangentSpace)$ 
   $p = projectVectorOnTo(Pos, TangentSpace)$ 
   $normalize(l); normalize(p)$ 
   $p_{per} = P \cdot C^{-1} \cdot M \cdot p_{obj}$ 
end for

```

As already mentioned in section 2.3.1, our light source is a directional light source (See figure 3.6).

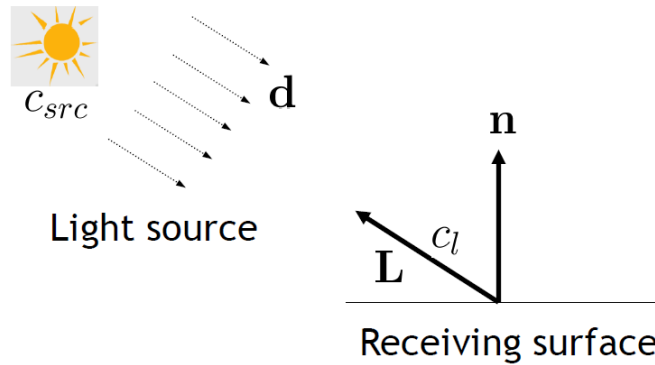


Figure 3.6: For a directional light source all light rays are in parallel.

3.3.2 Fragment Shader

The purpose of a fragment shader is to render per fragment. A fragment is spanned by three vertices of a given mesh. For each pixel within a fragment in the fragment shader, the output of from its spanning vertices computed in the vertex shaders 3.2 is trilinearly interpolated depending on the pixel's position within the fragment. Furthermore, there can be additional input be assigned which is not directly interpolated from the output of vertex shader programs. In our fragment shader 3.3 this will be: all the references to the image buffers, containing the Fourier images computed in Matlab 3.1, the number steps for

the Taylor approximation (in our shader 30), the minimal and maximal wavelength, scaling factors, a reference to a lookup table containing the CIE_{XYZ} color weights. Basically the whole computation within our fragment shader relies on the direction of light and the viewing direction. Our shader performs a numerical integration for our final derived expression in equation 2.31 using the trapezoidal-rule with uniform discretization of the wavelength spectrum at $5nm$ step sizes. This implies we are compressing sampled frequencies to the region near to the origin of their frequency domain due to the fact we are dividing the (u, v) by the wavelength and this implies that the (u, v) space is sampled non-linearly.

The Gaussian window approach derived in section 2.2.3 is performed for each discrete λ value using a window large enough to span $4\sigma_f$ in both dimensions. For precomputing DFT tables we generally use nanostructure height fields that span at least $65\mu m^2$ and are sampled with resolution of at least 100nm. This ensures that the spectral response encompasses all the wavelengths in the visible spectrum, i.e. from 380nm to 780nm.

Algorithm 3.3 Fragment diffraction shader pseudo code**INPUT:** *Precomputed DFT Terms, Scene Geometry***OUTPUT:** *StructuralColoronFragment*

```

1: Foreach Pixel  $p \in \text{Fragment}$  do
2:   INIT  $BRDF_{XYZ}, BRDF_{RGB}$  TO  $\text{vec4}(0.0)$ 
3:    $(u, v, w) = -\omega_i - \omega_r$ 
4:   for  $(\lambda = \lambda_{min}; \lambda \leq \lambda_{max}; \lambda = \lambda + \lambda_{step})$  do
5:      $xyzWeights = \text{ColorWeights}(\lambda)$ 
6:      $lookupCoord = \text{lookupCoord}(u, v, \lambda)$ 
7:     INIT  $P$  TO  $\text{vec2}(0.0)$ 
8:      $k = \frac{2\pi}{\lambda}$ 
9:     for  $(n = 0 \text{ TO } T)$  do
10:       $taylorScaleF = \frac{(kw)^n}{n!}$ 
11:      INIT  $F_{fft}$  TO  $\text{vec2}(0.0)$ 
12:       $anchorX = \text{int}(\text{floor}(\text{center}.x + \text{lookupCoord}.x * \text{fftImWidth}))$ 
13:       $anchorY = \text{int}(\text{floor}(\text{center}.y + \text{lookupCoord}.y * \text{fftImHeight}))$ 
14:      for  $(i = (anchorX - \text{winW}) \text{ TO } (anchorX + \text{winW}))$  do
15:        for  $(j = (anchorY - \text{winW}) \text{ TO } (anchorY + \text{winW}))$  do
16:           $dist = \text{distVecFromOriginTo}(i, j)$ 
17:           $pos = \text{localLookUp}(i, j, n)$ 
18:           $fftVal = \text{rescaledFourierValueAt}(pos)$ 
19:           $fftVal *= \text{gaussWeightOf}(dist)$ 
20:           $F_{fft} += fftVal$ 
21:        end for
22:      end for
23:       $P += taylorScaleF * F_{fft}$ 
24:    end for
25:     $xyzPixelColor += \text{dot}(\text{vec3}(|P|^2), xyzWeights)$ 
26:  end for
27:   $BRDF_{XYZ} = xyzPixelColor * C(\omega_i, \omega_r) * \text{shadowF}$ 
28:   $BRDF_{RGB}.xyz = D_{65} * M_{XYZ-RGB} * BRDF_{XYZ}.xyz$ 
29:   $BRDF_{RGB} = \text{gammaCorrect}(BRDF_{RGB})$ 
30: end for

```

From line 4 to 26:

This loop performs uniform sampling along wavelength-space. $\text{ColorWeights}(\lambda)$ computes the color weight for the current wavelength λ by linear interpolation between the color weight for $\lceil \lambda \rceil$ and $\lfloor \lambda \rfloor$ which are stored in an external weights-table (assuming this table contains wavelengths in 1nm steps). At line 6: $\text{lookupCoord}(u, v, \lambda)$ the coordinates for the texture lookup are computed - See 3.5. Line 25 sums up the diffraction color contribution for the current wavelength in iteration λ .

From line 9 to 24:

This loop performs the Taylor series approximation using T terms. Basically, the spectral response is approximated for our current (u, v, λ) . Furthermore, neighborhood boundaries for the gaussian-window sampling are computed, denoted as anchorX and anchorY.

From line 14 to 22:

In this inner most loop, the convolution of the gaussian window with the DFT of the patch is performed. *gaussWeightOf(dist)* computes the weights in equation (2.7) from the distance between the current pixel's coordinates and the current neighbor's position in texture space. Local lookup coordinates for the current fourier coefficient *fftVal* value are computed at line 17 and computed like described in 3.7. The actual texture lookup is performed at line 18 using those local coordinates. Inside *rescaledFourierValueAt* the values *fftVal* is rescaled by its extrema, i.e. $(fftVal * Max + Min)$ is computed, since *fftVal* is normalized 3.1. The current *fftVal* values in iteration is scaled by the current gaussian weight and then summed to the final neighborhood FFT contribution at line 20.

After line 26:

At line 27 the gain factor $C(\omega_i, \omega_r)$ 2.17 is multiplied by the current computed pixel color like formulated in 2.18. The gain factor contains the geometric term *refeq : geometricterm* and the Fresnel term *F*. We approximate *F* by the Schlick approximation *D.2*, using an reactive index at 1.5 since this is close to the measured value from snake sheds. Our BRDF values are scaled by a shadowing function as described in (SEE REFERENCES - PAPER), since most of the grooves in the snake skin nano-structures would form a V-cavity along the plane for a wave front with their top-edges at almost the same height.

Last, we transform our colors from the CIE_{XYZ} colorspace to the CIE_{RGB} space using the CIE Standard Illuminant D65, followed by a gamma correction. See 3.4.3 for further insight.

3.4 Technical details

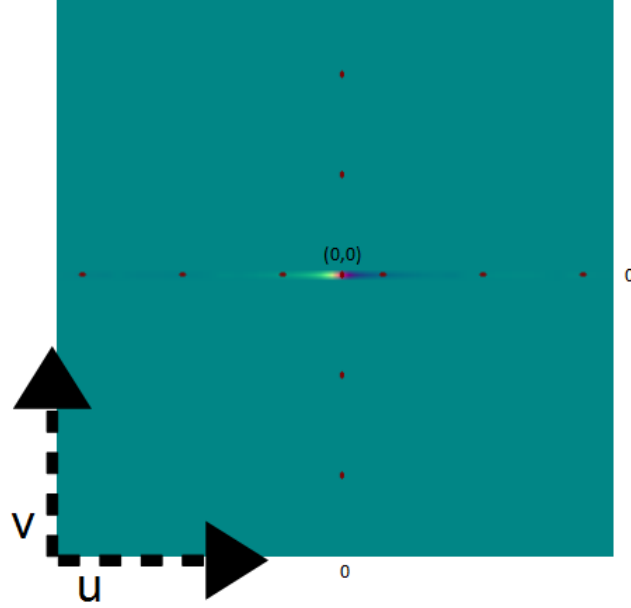
3.4.1 Texture lookup

In a GLSL shader the texture coordinates are normalized which means that the size of the texture maps to the coordinates on the range $[0, 1]$ in each dimension. By convention the the bottom left corner of an image has the coordinates $(0, 0)$, whereas the top right corner has the value $(1, 1)$ assigned.

Given a nano-scaled surface patch *P* with a resolution *A* by *A* microns stored as an *N* by *N* pixel image *I*. Then one pixel in any direction corresponds to $dH = \frac{A}{N} \mu m$. In Matlab we compute a series of *n* output images $\{I_{out_1}, \dots, I_{out_n}\}$ from *I*, which we will use for the lookup in our shader - See figure 3.7. For the lookup we use scaled and shifted (u, v) coordinates from ??.

Since the zero frequency component of output images was shifted towards the centre of each image, we have to shift *u*, *v* to the center of the current *N* by *N* pixel image by a bias *b*. Mathematically, the bias is a constant value is computed the following:

$$b = (N \% 2 == 0) \quad ? \quad \frac{N}{2} : \frac{N-1}{2} \quad (3.3)$$

Figure 3.7: (u, v) lookup image

For the scaling we have to think a little further: let's consider a T periodic signal in time, i.e. $x(t) = x(t + nT)$ for any integer n . After applying the DFT, we have its discrete spectrum $X[n]$ with frequency interval $w_0 = 2\pi/T$ and time interval t_0 . Let $k = \frac{2\pi}{\lambda}$ denote the wavenumber for the current wavelength λ . Then the signal is both periodic with time period T and discrete with time interval t_0 then its spectrum should be both discrete with frequency interval w_0 and periodic with frequency period $\Omega = \frac{2\pi}{t_0}$. This gives us the idea how to discretize the spectrum: Let us consider our Patch P assuming it is distributed as a periodic function on our surface. Then, its frequency interval along the x direction is $w_0 = \frac{2\pi}{T} = \frac{2\pi}{N \cdot dH}$. Thus only wave numbers that are integer multiples of w_0 after a multiplication with u must be considered, i.e. ku is integer multiple of w_0 . Hence the lookup for the u -direction will look like:

$$\frac{ku}{w_0} = \frac{kuNdH}{2\pi} \quad (3.4)$$

$$= \frac{uNdH}{\lambda} \quad (3.5)$$

Using those findings 3.3, 3.5, the final (u, v) texture lookup-coordinates for the current wavelength λ in iteration, will then look like:

$$(u_{lookup}, v_{lookup}) = \left(\frac{uNdH}{\lambda} + b, \frac{vNdH}{\lambda} + b \right) \quad (3.6)$$

Note for the windowing approach we are visiting a one pixel neighborhood for each pixel p . This is like a base change with (u_{lookup}, v_{lookup}) as new coordinate system origin. The lookup coordinates for the neighbor-pixel (i, j) are:

$$(u_{lookup}, v_{lookup}) = (i, j) - (u_{lookup}, v_{lookup}) \quad (3.7)$$

3.4.2 Texture Blending

The final rendered color for each pixel is a weighted average of different color components, such as the diffraction color, the texture color and the diffuse color. In our shader the diffraction color is weighted by a constant $w_{diffuse}$. the texture color is once scales by a binary weight determined by the absolute value of the Fresnel Term F and once by $1 - w_{diffuse}$.

Algorithm 3.4 Texture Blending

$\alpha = (abs(F) > 1)?1 : 0$
 $c_{out} = (1 - w_{diffuse}) * c_{diffraction} + (1 - \alpha) * c_{texture} + w_{diffuse} * c_{texture}$

3.4.3 Color Transformation

In our shader we access a table which contains precomputed CIE's color matching functions values from $\lambda_{min} = 380nm$ to $\lambda_{max} = 780nm$ in $5nm$ steps. Such a function value table can be found at downloaded at cvrl.ioo.ucl.ac.uk for example. We compute the (X, Y, Z) CIE_{XYZ} color values as described in ??.

We can transform the color values into CIE_{RGB} by performing the following linear transformation:

$$\begin{bmatrix} R \\ G \\ B \end{bmatrix} = M \cdot \begin{bmatrix} X \\ Y \\ Z \end{bmatrix} \quad (3.8)$$

where one possible transformation is:

$$M = \begin{bmatrix} 0.41847 & -0.15866 & -0.082835 \\ -0.091169 & 0.25243 & 0.015708 \\ 0.00092090 & -0.0025498 & 0.17860 \end{bmatrix} \quad (3.9)$$

There are some other color space transformation. The shader uses the CIE Standard Illuminant D65 which is intended to represent average daylight. Using D65 the whole colorspace transformation will look like:

$$\begin{bmatrix} R \\ G \\ B \end{bmatrix} = M \cdot \begin{bmatrix} X \cdot D65.x \\ Y \cdot D65.y \\ Z \cdot D65.z \end{bmatrix} \quad (3.10)$$

Last we perform gamma correction on each pixel's (R, G, B) value. Gamma correction is a non linear transformation which controls the overall brightness of an image.

3.5 Discussion

The fragment shader algorithm described in 3.3 performs the gaussian window approach by sampling over the whole wavelength spectrum in uniform step sizes.

This algorithm is valid but also slow since we iterate for each pixel over the whole lambda spectrum. Furthermore, for any pixel, we iterate over its 1 neighborhood. Considering the loop for the taylor approximation as well, we will have a run-time complexity of $O(\#spectrtumIter \cdot \#taylorIter \cdot neighborhoodRadius^2)$. Hence, Instead sampling over the whole wavelength spectrum, we could instead integrate over just a few required lambdas which are elicited like the following: Lets consider (u, v, w) defined as ???. Let d be the spacing between two slits of a grating. For any $L(\lambda) \neq 0$ it follows $\lambda_n^u = \frac{du}{n}$ and $\lambda_n^v = \frac{dv}{n}$. For $n = 0$ there it follows $(u, v) = (0, 0)$. If $u, v > 0$

$$N_{min}^u = \frac{du}{\lambda_{max}} \leq n_u \leq \frac{du}{\lambda_{min}} = N_{min}^u$$

$$N_{min}^v = \frac{dv}{\lambda_{max}} \leq n_v \leq \frac{dv}{\lambda_{min}} = N_{min}^v$$

If $u, v < 0$

$$N_{min}^u = \frac{du}{\lambda_{min}} \leq n_u \leq \frac{du}{\lambda_{min}} = N_{max}^u$$

$$N_{min}^v = \frac{dv}{\lambda_{min}} \leq n_v \leq \frac{dv}{\lambda_{min}} = N_{max}^v$$

By transforming those equation to $(\lambda_{min}^u, \lambda_{min}^u)$, $(\lambda_{min}^v, \lambda_{min}^v)$ respectively for any (u, v, w) for each pixel we can reduce the total number of required iterations in our shader.

Another variant is the *PQ* approach described in chapter 2 2.6.1. Depending on the interpolation method, there are two possible variants we can think of as described in 2.6.2. Either we try to interpolate linearly or use sinc interpolation. The first variant does not require to iterate over a pixel's neighborhood, it is also faster than the gaussian window approach. One could think of a combination of those two optimization approaches. Keep in mind, both of these approaches are further approximation. The quality of the rendered images will suffer using those two approaches. The second variant, using the sinc function interpolation is well understood in the field of signal processing and will give us reliable results. The drawback of this approach is that we again have to iterate over a neighborhood within the fragment shader which will slow down the whole shading. The following algorithm describes the modification of the fragment shader 3.3 in order to use sinc interpolation for the pq approach 2.6.1.

Algorithm 3.5 Sinc interpolation for pq approach

```

Foreach Pixel  $p \in Image I$  do
   $w_p = \sum_{(i,j) \in \mathcal{N}_1(p)} sinc(\Delta_{p,(i,j)} \cdot \pi + \epsilon) \cdot I(i, j)$ 
   $c_p = w_p \cdot (p^2 + q^2)^{\frac{1}{2}}$ 
   $render(c_p)$ 
end for

```

In a fragment shader we compute for each pixel p in the current fragment its reconstructed function value $f(p)$ stores in w_p . w_p is the reconstructed signal value at $f(p)$ by the sinc function as described in 2.6.2. We calculate

the distance $\Delta_{p,(i,j)}$ between the current pixel p and each of its neighbor pixels $(i,j) \in \mathcal{N}_1(p)$ in its one-neighborhood. Multiplying this distance by π gives us the an angle used for the sinc function interpolation. We add a small integer ϵ in order to avoid division by zeros side-effects.

Appendix A

Signal Processing Basics

A signal is a function that conveys information about the behavior or attributes of some phenomenon. In the physical world, any quantity exhibiting variation in time or variation in space (such as an image) is potentially a signal that might provide information on the status of a physical system, or convey a message between observers.

The Fourier Transform is an important image processing tool which is used to decompose an image into its sine and cosine components. The output of the transformation represents the image in the Fourier or frequency domain, while the input image is the spatial domain equivalent. In the Fourier domain image, each point represents a particular frequency contained in the spatial domain image.

A.1 Fourier Transformation

The Fourier-Transform is a mathematical tool which allows to transform a given function or rather a given signal from defined over a time- (or spatial-) domain into its corresponding frequency-domain.

Let f an measurable function over \mathbb{R}^n . Then, the continuous Fourier Transformation (**FT**), denoted as $\mathcal{F}\{f\}$ of f , ignoring all constant factors in the formula, is defined as:

$$\mathcal{F}_{FT}\{f\}(w) = \int_{\mathbb{R}^n} f(x)e^{-iwt}dt \quad (\text{A.1})$$

whereas its inverse transform is defined like the following which allows us to obtain back the original signal:

$$\mathcal{F}_{FT}^{-1}\{f\}(w) = \int_{\mathbb{R}} \mathcal{F}\{w\}e^{iwt}dt \quad (\text{A.2})$$

Usual w is identified by the angular frequency which is equal $w = \frac{2\pi}{T} = 2\pi v_f$. In this connection, T is the period of the resulting spectrum and v_f is its corresponding frequency.

By using Fourier Analysis, which is the approach to approximate any function by sums of simpler trigonometric functions, we gain the so called Discrete Time Fourier Transform (in short **DTFT**). The DTFT operates on a discrete

function. Usually, such an input function is often created by digitally sampling a continuous function. The DTFT itself is operation on a discretized signal on a continuous, periodic frequency domain and looks like the following:

$$\mathcal{F}_{DTFT}\{f\}(w) = \sum_{-\infty}^{\infty} f(x)e^{-iwx} \quad (\text{A.3})$$

Note that the DTFT is not practically suitable for digital signal processing since there a signal can be measured only in a finite number of points. Thus, we can further discretize the frequency domain and will get then the Discrete Fourier Transformation (in short **DFT**) of the input signal:

$$\mathcal{F}_{DFT}\{f\}(w) = \sum_{n=0}^{N-1} f(x)e^{-iwn} \quad (\text{A.4})$$

Where the angular frequency w_n is defined like the following $w_n = \frac{2\pi n}{N}$ and N is the number of samples within an equidistant period sampling.

Any continuous function $f(t)$ can be expressed as a series of sines and cosines. This representation is called the Fourier Series (denoted by *FS*) of $f(t)$.

$$f(t) = \frac{1}{2}a_0 + \sum_{n=1}^{\infty} a_n \cos(nt) + \sum_{n=1}^{\infty} b_n \sin(nt) \quad (\text{A.5})$$

where

$$\begin{aligned} a_0 &= \int_{-\pi}^{\pi} f(t)dt \\ a_n &= \frac{1}{\pi} \int_{-\pi}^{\pi} f(t)\cos(nt)dt \\ b_n &= \frac{1}{\pi} \int_{-\pi}^{\pi} f(t)\sin(nt)dt \end{aligned} \quad (\text{A.6})$$

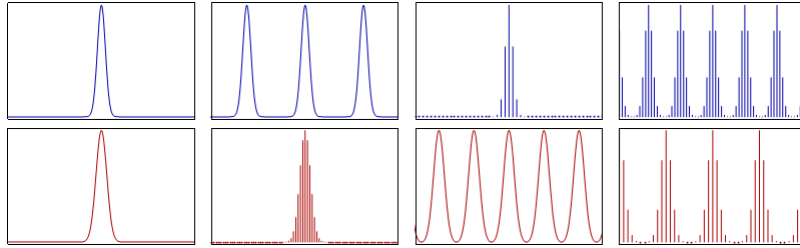


Figure A.1: Relationship¹ between the continuous Fourier transform and the discrete Fourier transform: Left column: A continuous function (top) and its Fourier transform A.1 (bottom). Center-left column: Periodic summation of the original function (top). Fourier transform (bottom) is zero except at discrete points. The inverse transform is a sum of sinusoids called Fourier series A.5. Center-right column: Original function is discretized (multiplied by a Dirac comb) (top). Its Fourier transform (bottom) is a periodic summation (DTFT) of the original transform. Right column: The DFT A.4 (bottom) computes discrete samples of the continuous DTFT A.3. The inverse DFT (top) is a periodic summation of the original samples.

Spetail signal $f(t)$ is	Operator	Transformed frequency signal $\hat{f}(\omega)$ is
continuous and periodic in t	FS A.5	only discrete in ω
only continuous in t	FT A.1	only continuous in ω
only discrete in t	DTFT A.3	continuous and periodic in ω
discrete and periodic in t	DFT A.4	discrete and periodic in ω

Table A.1: Fourier operator to apply for a given spatial input signal and the properties of its resulting output signal in frequency space

A.2 Convolution

The convolution $f * g$ of two functions $f, g: \mathbb{R}^n \rightarrow \mathbb{C}$ is defined as:

$$(f * g)(t) = \int_{\mathbb{R}^n} f(t)g(t - x)dx \quad (\text{A.7})$$

Note that the Fourier transform of the convolution of two functions is the product of their Fourier transforms. This is equivalent to the fact that Convolution in spatial domain is equivalent to multiplication in frequency domain. Therefore, the inverse Fourier transform of the product of two Fourier transforms is the convolution of the two inverse Fourier transforms. Last an illustration of the relationships between the previous presented Fourier transformations and different given input signals. First an concrete example shown in Figure A.1. Table A.1 tells what Fourier transformation operator has to be applied to which kind of input signal and what properties its resulting Fourier transform will have.

A.3 Taylor Series

Taylor series is a representation of a function as an infinite sum of terms that are calculated from the values of the function's derivatives at a single point.

The Taylor series \mathcal{T} of a real or complex-valued function $f(x)$ that is infinitely differentiable at a real or complex number a is the power series:

$$\mathcal{T}(f; a)(x) = \sum_{n=0}^{\infty} \frac{f^n(a)}{n!} (x - a)^n \quad (\text{A.8})$$

¹image of illustration has been taken from wikipedia

Appendix B

Summary of Stam's Derivations

In his paper about Diffraction Shader, J. Stam derives a BRDF which is modeling the effect of diffraction for various analytical anisotropic reflexion models relying on the so called scalar wave theory of diffraction for which a wave is assumed to be a complex valued scalar. It's noteworthy, that Stam's BRDF formulation does not take into account the polarization of the light. Fortunately, light sources like sunlight and light bulbs are unpolarized.

A further assumption in Stam's Paper is, the emanated waves from the source are stationary, which implies the wave is a superposition of independent monochromatic waves. This implies that each wave is associated to a definite wavelength λ . However, sunlight once again fulfills this fact.

In our simulations we will always assume we have given a directional light source, i.e. sunlight. Hence, Stam's model can be used for our derivations.

For his derivations Stam uses the Kirchhoff integral¹, which is relating the reflected field to the incoming field. This equation is a formalization of Huygen's well-known principle that states that if one knows the wavefront at a given moment, the wave at a later time can be deduced by considering each point on the first wave as the source of a new disturbance. Mathematically speaking, once the field $\psi_1 = e^{ik\mathbf{x}\cdot\mathbf{ss}}$ on the surface is known, the field ψ_2 everywhere else away from the surface can be computed. More precisely, we want to compute the wave ψ_2 equal to the reflection of an incoming planar monochromatic wave $\psi_1 = e^{ik\omega_i\cdot\mathbf{x}}$ traveling in the direction ω_i from a surface S to the light source. Formally, this can be written as:

$$\psi_2(\omega_i, \omega_r) = \frac{ike^{iKR}}{4\pi R} (F(-\omega_i - \omega_r) - (-\omega_i + \omega_r)) \cdot I_1(\omega_i, \omega_r) \quad (\text{B.1})$$

with

$$I_1(\omega_i, \omega_r) = \int_S \hat{\mathbf{n}} e^{ik(-\omega_i - \omega_r) \cdot \mathbf{s}} d\mathbf{s} \quad (\text{B.2})$$

¹See http://en.wikipedia.org/wiki/Kirchhoff_integral_theorem for further information.

In applied optics, when dealing with scattered waves, one does use differential scattering cross-section rather than defining a BRDF which has the following identity:

$$\sigma^0 = 4\pi \lim_{R \rightarrow \infty} R^2 \frac{\langle |\psi_2|^2 \rangle}{\langle |\psi_1|^2 \rangle} \quad (\text{B.3})$$

where R is the distance from the center of the patch to the receiving point x_p , $\hat{\mathbf{n}}$ is the normal of the surface at s and the vectors:

The relationship between the BRDF and the scattering cross section can be shown to be equal to

$$BRDF = \frac{1}{4\pi} \frac{1}{A} \frac{\sigma^0}{\cos(\theta_i) \cos(\theta_r)} \quad (\text{B.4})$$

where θ_i and θ_r are the angles of incident and reflected directions on the surface with the surface normal \mathbf{n} . See ??.

The components of vector resulting by the difference between these direction vectors: In order to simplify the calculations involved in his vectorized integral equations, Stam considers the components of vector

$$(u, v, w) = -\omega_i - \omega_r \quad (\text{B.5})$$

explicitly and introduces the equation:

$$I(ku, kv) = \int_S \hat{\mathbf{n}} e^{ik(u,v,w) \cdot \mathbf{s}} d\mathbf{s} \quad (\text{B.6})$$

which is a first simplification of B.2. Note that the scalar w is the third component of ?? and can be written as $w = -(\cos(\theta_i) + \cos(\theta_r))$ using spherical coordinates. The scalar $k = \frac{2\pi}{\lambda}$ represent the wavenumber.

During his derivations, Stam provides a analytical representation for the Kirchhoff integral assuming that each surface point $s(x, y)$ can be parameterized by $(x, y, h(x, y))$ where h is the height at the position (x, y) on the given (x, y) surface plane. Using the tangent plane approximation for the parameterized surface and plugging it into B.6 he will end up with:

$$\mathbf{I}(ku, kv) = \int \int (-h_x(x, y), -h_y(x, y), 1) e^{ikwh(x, y)} e^{ik(ux+vy)} dx dy \quad (\text{B.7})$$

For further simplification Stam formulates auxillary function which depends on the provided height field:

$$p(x, y) = e^{iwh(x, y)} \quad (\text{B.8})$$

which will allow him to further simplify his equation B.7 to:

$$\mathbf{I}(ku, kv) = \int \int \frac{1}{ikw} (-p_x, -p_y, ikwp) dx dy \quad (\text{B.9})$$

where he used that $(-h_x(x, y), -h_y(x, y), 1) e^{ikwh(x, y)}$ is equal to $\frac{(-p_x, -p_y, ikwp)}{ikw}$ using the definition of the partial derivatives applied to the function ??.

Let $P(x, y)$ denote the Fourier Transform (FT) of $p(x, y)$. Then, the differentiation with respect to x respectively to y in the Fourier domain is equivalent to a multiplication of the Fourier transform by $-iku$ or $-ikv$ respectively. This leads him to the following simplification for B.7:

$$\mathbf{I}(ku, kv) = \frac{1}{w} P(ku, kv) \cdot (u, v, w) \quad (\text{B.10})$$

Let us consider the term $g = (F(-\omega_i - \omega_r) - (-\omega_i + \omega_r))$, which is a scalar factor of B.1. The dot product with g and $(-\omega_i - \omega_r)$ is equal $2F(1 + \omega_i \cdot \omega_r)$. Putting this finding and the identity B.10 into B.1 he will end up with:

$$\psi_2(\omega_i, \omega_r) = \frac{ike^{iKR}}{4\pi R} \frac{2F(1 + \omega_i \cdot \omega_r)}{w} P(ku, kv) \quad (\text{B.11})$$

By using the identity B.4, this will lead us to his main finding:

$$BRDF_\lambda(\omega_i, \omega_r) = \frac{k^2 F^2 G}{4\pi^2 A w^2} \langle |P(ku, kv)|^2 \rangle \quad (\text{B.12})$$

where G is the so called geometry term which is equal:

$$G = \frac{(1 + \omega_i \cdot \omega_r)^2}{\cos(\theta_i) \cos(\theta_r)} \quad (\text{B.13})$$

Appendix C

Summary of Stam's Derivations

C.1 Taylor Series Approximation

For an $N \in \mathbb{N}$ such that

$$\sum_{n=0}^N \frac{(ikwh)^n}{n!} \mathcal{F}\{h^n\}(\alpha, \beta) \approx P(\alpha, \beta) \quad (\text{C.1})$$

we have to prove:

1. Show that there exist such an $N \in \mathbb{N}$ s.t the approximation holds true.
2. Find a value for B s.t. this approximation is below a certain error bound, for example machine precision ϵ .

C.1.1 Proof Sketch of 1.

By the **ratio test** (see [1]) It is possible to show that the series $\sum_{n=0}^N \frac{(ikwh)^n}{n!} \mathcal{F}\{h^n\}(\alpha, \beta)$ converges absolutely:

Proof: Consider $\sum_{k=0}^{\infty} \frac{y^k}{k!}$ where $a_k = \frac{y^k}{k!}$. By applying the definition of the ratio test for this series it follows:

$$\forall y : \limsup_{k \rightarrow \infty} \left| \frac{a_{k+1}}{a_k} \right| = \limsup_{k \rightarrow \infty} \frac{y}{k+1} = 0 \quad (\text{C.2})$$

Thus this series converges absolutely, no matter what value we will pick for y.

C.1.2 Part 2: Find such an N

Let $f(x) = e^x$. We can formulate its Taylor-Series, stated above. Let $P_n(x)$ denote the n-th Taylor polynom,

$$P_n(x) = \sum_{k=0}^n \frac{f^{(k)}(a)}{k!} (x-a)^k \quad (\text{C.3})$$

where a is our developing point (here a is equal zero).

We can define the error of the n -th Taylor polynomial to be $E_n(x) = f(x) - P_n(x)$. the error of the n -th Taylor polynomial is difference between the value of the function and the Taylor polynomial This directly implies $|E_n(x)| = |f(x) - P_n(x)|$. By using the Lagrangian Error Bound it follows:

$$|E_n(x)| \leq \frac{M}{(n+1)!} |x - a|^{n+1} \quad (C.4)$$

with $a = 0$, where M is some value satisfying $|f^{(n+1)}(x)| \leq M$ on the interval $I = [a, x]$. Since we are interested in an upper bound of the error and since a is known, we can reformulate the interval as $I = [0, x_{max}]$, where

$$x_{max} = \|i\| k_{max} w_{max} h_{max} \quad (C.5)$$

We are interested in computing an error bound for $e^{ikwh(x,y)}$. Assuming the following parameters and facts used within Stam's Paper:

- Height of bump: 0.15micro meters
- Width of a bump: 0.5micro meters
- Length of a bump: 1micro meters
- $k = \frac{2\pi}{\lambda}$ is the wavenumber, $\lambda \in [\lambda_{min}, \lambda_{max}]$ and thus $k_{max} = \frac{2\pi}{\lambda_{min}}$. Since $(u, v, w) = -\omega_i - \omega_r$ and both are unit direction vectors, each component can have a value in range $[-2, 2]$.
- for simplification, assume $[\lambda_{min}, \lambda_{max}] = [400nm, 700nm]$.

We get:

$$\begin{aligned} x_{max} &= \|i\| * k_{max} * w_{max} * h_{max} \\ &= k_{max} * w_{max} * h_{max} \\ &= 2 * \left(\frac{2\pi}{4 * 10^{-7}m} \right) * 1.5 * 10^{-7} \\ &= 1.5\pi \end{aligned} \quad (C.6)$$

and it follows for our interval $I = [0, 1.5\pi]$.

Next we are going to find the value for M . Since the exponential function is monotonically growing (on the interval I) and the derivative of the **exp** function is the exponential function itself, we can find such an M :

$$\begin{aligned} M &= e^{x_{max}} \\ &= \exp(1.5\pi) \end{aligned}$$

and $|f^{(n+1)}(x)| \leq M$ holds. With

$$\begin{aligned} |E_n(x_{max})| &\leq \frac{M}{(n+1)!} |x_{max} - a|^{n+1} \\ &= \frac{\exp(1.5\pi) * (1.5\pi)^{n+1}}{(n+1)!} \end{aligned} \quad (C.7)$$

we now can find a value of n for a given bound, i.e. we can find an value of $N \in \mathbb{N}$ s.t. $\frac{\exp(1.5\pi) * (1.5\pi)^{N+1}}{(N+1)!} \leq \epsilon$. With Octave/Matlab we can see:

- if $N=20$ then $\epsilon \approx 2.9950 * 10^{-4}$
- if $N=25$ then $\epsilon \approx 8.8150 * 10^{-8}$
- if $N=30$ then $\epsilon \approx 1.0050 * 10^{-11}$

With this approach we have that $\sum_{n=0}^{25} \frac{(ikwh)^n}{n!} \mathcal{F}\{h^n\}(\alpha, \beta)$ is an approximation of $P(u, v)$ with error $\epsilon \approx 8.8150 * 10^{-8}$. This means we can precompute 25 Fourier Transformations in order to approximate $P(u, v)$ having an error $\epsilon \approx 8.8150 * 10^{-8}$.

C.2 PQ approach

C.2.1 One dimensional case

Since our series is bounded, we can simplify the right-hand-side of equation 2.36.

Note that e^{-ix} is a complex number. Every complex number can be written in its polar form, i.e.

$$e^{-ix} = \cos(x) + i\sin(x) \quad (\text{C.8})$$

Using the following trigonometric identities

$$\begin{aligned} \cos(-x) &= \cos(x) \\ \sin(-x) &= -\sin(x) \end{aligned} \quad (\text{C.9})$$

combined with C.8 we can simplify the series 2.36 even further to:

$$\frac{1 - e^{iwT(N+1)}}{1 - e^{-iwT}} = \frac{1 - \cos(wT(N+1)) + i\sin(wT(N+1))}{1 - \cos(wT) + i\sin(wT)} \quad (\text{C.10})$$

Equation C.10 is still a complex number, denoted as $(p + iq)$. Generally, every complex number can be written as a fraction of two complex numbers. This implies that the complex number $(p + iq)$ can be written as $(p + iq) = \frac{(a+ib)}{(c+id)}$ for any $(a + ib), (c + id) \neq 0$. Let us use the following substitutions:

$$\begin{aligned} a &:= 1 - \cos(wT(N+1)) & b &= \sin(wT(N+1)) \\ c &= 1 - \cos(wT) & d &= \sin(wT) \end{aligned} \quad (\text{C.11})$$

Hence, using C.11, it follows

$$\frac{1 - e^{iwT(N+1)}}{1 - e^{-iwT}} = \frac{(a + ib)}{(c + id)} \quad (\text{C.12})$$

By rearranging the terms, it follows $(a + ib) = (c + id)(p + iq)$ and by multiplying its right hand-side out we get the following system of equations:

$$\begin{aligned}(cp - dq) &= a \\ (dp + cq) &= b\end{aligned}\tag{C.13}$$

After multiplying the first equation of C.13 by c and the second by d and then adding them together, we get using the law of distributivity new identities for p and q :

$$\begin{aligned}p &= \frac{(ac + bd)}{c^2 + d^2} \\ q &= \frac{(bc + ad)}{c^2 + d^2}\end{aligned}\tag{C.14}$$

Using some trigonometric identities and putting our substitution from C.11 for a, b, c, d back into the current representation C.14 of p and q we will get:

$$\begin{aligned}p &= \frac{1}{2} + \frac{1}{2} \left(\frac{\cos(wTN) - \cos(wT(N+1))}{1 - \cos(wT)} \right) \\ q &= \frac{\sin(wT(N+1)) - \sin(wTN) - \sin(wT)}{2(1 - \cos(wT))}\end{aligned}\tag{C.15}$$

Since we have seen, that $\sum_{n=0}^N e^{-uwnT}$ is a complex number and can be written as $(p + iq)$, we now know an explicit expression for p and q . Therefore, the one dimensional inverse Fourier transform of S is equal:

$$\begin{aligned}\mathcal{F}^{-1}\{S\}(w) &= \mathcal{F}^{-1}\{f\}(w) \sum_{n=0}^N e^{-iwnT} \\ &= (p + iq)\mathcal{F}^{-1}\{f\}(w)\end{aligned}\tag{C.16}$$

C.2.2 Two dimensional case

$$\begin{aligned}
\mathcal{F}^{-1}\{S\}(w_1, w_2) &= \int_{-\infty}^{\infty} \int_{-\infty}^{\infty} \sum_{n_2=0}^{N_1} \sum_{n_2=0}^{N_2} h(x_1 + n_1 T_1, x_2 + n_2 T_2) e^{i w(x_1 + x_2)} dx_1 dx_2 \\
&= \int_{-\infty}^{\infty} \int_{-\infty}^{\infty} \sum_{n_2=0}^{N_1} \sum_{n_2=0}^{N_2} h(y_1, y_2) e^{i w((y_1 - n_1 T_1) + (y_2 + n_2 T_2))} dy_1 dy_2 \\
&= \sum_{n_2=0}^{N_1} \sum_{n_2=0}^{N_2} \int_{-\infty}^{\infty} \int_{-\infty}^{\infty} h(y_1, y_2) e^{i w(y_1 + y_2)} e^{-i w(n_1 T_1 + n_2 T_2)} dy_1 dy_2 \\
&= \sum_{n_2=0}^{N_1} \sum_{n_2=0}^{N_2} e^{-i w(n_1 T_1 + n_2 T_2)} \int_{-\infty}^{\infty} \int_{-\infty}^{\infty} \text{Box}(y_1, y_2) e^{i w(y_1 + y_2)} dy_1 dy_2 \\
&= \left(\sum_{n_2=0}^{N_1} \sum_{n_2=0}^{N_2} e^{-i w(n_1 T_1 + n_2 T_2)} \right) \mathcal{F}^{-1}\{h\}(w_1, w_2) \\
&= \left(\sum_{n_2=0}^{N_1} e^{-i w n_1 T_1} \right) \left(\sum_{n_2=0}^{N_2} e^{-i w n_2 T_2} \right) \mathcal{F}^{-1}\{h\}(w_1, w_2) \\
&= (p_1 + i q_1)(p_2 + i q_2) \mathcal{F}^{-1}\{h\}(w_1, w_2) \\
&= ((p_1 p_2 - q_1 q_2) + i(p_1 p_2 + q_1 q_2)) \mathcal{F}^{-1}\{h\}(w_1, w_2) \\
&= (p + i q) \mathcal{F}_{DFTT}\{h\}(w_1, w_2) \tag{C.17}
\end{aligned}$$

Where we have defined

$$\begin{aligned}
p &:= (p_1 p_2 - q_1 q_2) \\
q &:= (p_1 p_2 + q_1 q_2) \tag{C.18}
\end{aligned}$$

Appendix D

Appendix

D.1 The 3rd component w

From the definition ?? of $(u, v, w) = -\omega_i - \omega_r$ and using spherical coordinates D.3, we get for w the following identity:

$$\begin{aligned} w &= -\omega_i - \omega_r \\ &= -(\omega_i + \omega_r) \\ &= -(\cos(\theta_i) + \cos(\theta_r)) \end{aligned} \tag{D.1}$$

and therefore w^2 is equal $(\cos(\theta_i) + \cos(\theta_r))^2$.

D.2 Schlick's approximation

The Fresnel's equations describe the reflection and transmission of electromagnetic waves at an interface. That is, they give the reflection and transmission coefficients for waves parallel and perpendicular to the plane of incidence. Schlick's approximation is a formula for approximating the contribution of the Fresnel term where the specular reflection coefficient R can be approximated by:

$$R(\theta) = R_0 + (1 - R_0)(1 - \cos \theta)^5 \tag{D.2}$$

and

$$R_0 = \left(\frac{n_1 - n_2}{n_1 + n_2} \right)^2$$

where θ is the angle between the viewing direction and the half-angle direction, which is halfway between the incident light direction and the viewing direction, hence $\cos \theta = (H \cdot V)$. And n_1, n_2 are the indices of refraction of the two medias at the interface and R_0 is the reflection coefficient for light incoming parallel to the normal (i.e., the value of the Fresnel term when $\theta = 0$ or minimal reflection). In computer graphics, one of the interfaces is usually air, meaning that n_1 very well can be approximated as 1.

D.3 Spherical Coordinates

$$\forall \begin{pmatrix} x \\ y \\ z \end{pmatrix} \in \mathbb{R}^3 : \exists r \in [0, \infty) \exists \phi \in [0, 2\pi] \exists \theta \in [0, \pi] \text{ s.t.}$$

$$\begin{pmatrix} x \\ y \\ z \end{pmatrix} = \begin{pmatrix} r \sin(\theta) \cos(\phi) \\ r \sin(\theta) \sin(\phi) \\ r \cos(\theta) \end{pmatrix}$$

D.4 Tangent Space

The concept of tangentspace-transformation of tangent space is used in order to convert a point between world and tangent space. GLSL fragment shaders require normals and other vertex primitives declared at each pixel point, which mean that we have one normal vector at each texel and the normal vector axis will vary for every texel.

Think of it as a bumpy surface defined on a flat plane. If those normals were declared in the world space coordinate system, we would have to rotate these normals every time the model is rotated, even when just for a small amount. Since the lights, cameras and other objects are usually defined in world space coordinate system, and therefore, when they are involved in an calculation within the fragment shader, we would have to rotate them as well for every pixel. This would involve almost countless many object to world matrix transformations need to take place at the pixel level. Therefore, instead doing so, we transform all vertex primitives into tangent space within the vertex shader.

To make this point clear an example: Even we would rotate the cube in figure D.1, the tangent space axis will remain aligned with respect to the face. Which practically speaking, will save us from performing many space transformations applied pixel-wise within the fragment shader and instead allows us to perform us the tangentspace transformation of every involved vertex primitive in the vertex-shader.

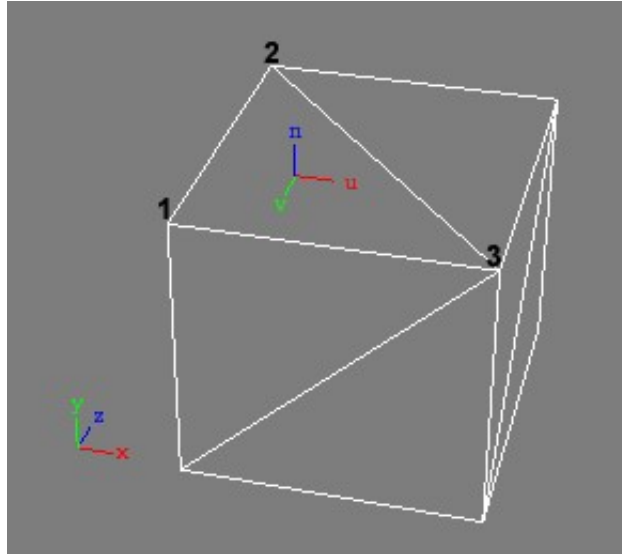


Figure D.1: Cube in world space (x, y, z) showing the tangen space (u, v, n) of its face $(2, 1, 3)$

List of Tables

A.1	Fourier operator to apply for a given spatial input signal and the properties of its resulting output signal in frequency space	41
-----	---	----

List of Figures

1.1	Example of Biological Color Production	1
1.2	Structural color examples	2
1.3	Xenopeltis AFM image	3
2.1	Problem Statement	7
2.2	Problem Statement: Output	8
2.3	FT by DTFT	9
2.4	Coherence Area using Gaussian Window	10
2.5	DTFT by DFT	11
2.6	Comparission between a given random one dimensional input signal $s(t)$ and its sinc interpolation $\hat{s}(t)$. Notice that for the interpolation there were $N = 100$ samples from the original signal provided.	22
3.1	Blaze	27
3.2	Renderer Architecture	28
3.3	A wireframe mesh represents an object as a set of faces and a set of vertices.	29
3.4	Camera coordinate system where its origin defines the center of projection of camera	30
3.5	Illustration of involved components in order to construct the camera matrix. We introduce some helper vectors $z_c = \frac{e-d}{ e-d }$, $x_c = \frac{up \times z_c}{ up \times z_c }$ and $z_c \times x_c$ for the actual construction of the camera matrix	30
3.6	For a directional light source all light rays are in parallel.	31
3.7	(u, v) lookup image	35
D.1	Cube in world space (x, y, z) showing the tangen space (u, v, n) of its face $(2, 1, 3)$	52

List of Algorithms

3.1	Precomputation: Pseudo code to generate Fourier terms	26
3.2	Vertex diffraction shader pseudo code	31
3.3	Fragment diffraction shader pseudo code	33
3.4	Texture Blending	36
3.5	Sinc interpolation for pq approach	37

Bibliography

- [Bar07] BARTSCH, Hans-Jochen: *Taschenbuch Mathematischer Formeln*. 21th edition. HASNER, 2007. – ISBN 978–3–8348–1232–2
- [CT12] CUYPERS T., et a.: Reflectance Model for Diffraction. In: *ACM Trans. Graph.* 31, 5 (2012), September
- [DSD14] D. S. DHILLON, et a.: Interactive Diffraction from Biological Nanostructures. In: *EUROGRAPHICS 2014/ M. Paulin and C. Dachsbacher* (2014), January
- [For11] FORSTER, Otto: *Analysis 3*. 6th edition. VIEWEG+TEUBNER, 2011. – ISBN 978–3–8348–1232–2
- [I.N14] I.NEWTON: *Opticks, reprinted*. CreateSpace Independent Publishing Platform, 2014. – ISBN 978–1499151312
- [JG04] JUAN GUARDADO, NVIDIA: Simulating Diffraction. In: *GPU Gems* (2004). <https://developer.nvidia.com/content/gpu-gems-chapter-8-simulating-diffraction>
- [LM95] LEONARD MANDEL, Emil W.: *Optical Coherence and Quantum Optics*. Cambridge University Press, 1995. – ISBN 978–0521417112
- [MT10] MATIN T.R., et a.: Correlating Nanostructures with Function: Structural Colors on the Wings of a Malaysian Bee. (2010), August
- [PAT09] PAUL A. TIPLER, Gene M.: *Physik für Wissenschaftler und Ingenieure*. 6th edition. Spektrum Verlag, 2009. – ISBN 978–3–8274–1945–3
- [PS09] P. SHIRLEY, S. M.: *Fundamentals of Computer Graphics*. 3rd edition. A K Peters, Ltd, 2009. – ISBN 978–1–56881–469–8
- [R.H12] R.HOOKE: *Micrographia, reprinted*. CreateSpace Independent Publishing Platform, 2012. – ISBN 978–1470079031
- [RW11] R. WRIGHT, et a.: *OpenGL SuperBible*. 5th edition. Addison-Wesley, 2011. – ISBN 978–0–32–171261–5
- [Sta99] STAM, J.: Diffraction Shaders. In: *SIGGRAPH 99 Conference Proceedings* (1999), August
- [T.Y07] T.YOUNG: *A course of lectures on natural philosophy and the mechanical arts Volume 1 and 2*. Johnson, 1807, 1807

Erklärung

gemäss Art. 28 Abs. 2 RSL 05

Name/Vorname:

Matrikelnummer:

Studiengang:

Bachelor ☐ Master ☐ Dissertation ☐

Titel der Arbeit:

.....

.....

LeiterIn der Arbeit:

.....

Ich erkläre hiermit, dass ich diese Arbeit selbständig verfasst und keine anderen als die angegebenen Quellen benutzt habe. Alle Stellen, die wörtlich oder sinngemäss aus Quellen entnommen wurden, habe ich als solche gekennzeichnet. Mir ist bekannt, dass andernfalls der Senat gemäss Artikel 36 Absatz 1 Buchstabe o des Gesetzes vom 5. September 1996 über die Universität zum Entzug des auf Grund dieser Arbeit verliehenen Titels berechtigt ist.

.....

Ort/Datum

.....

Unterschrift